IEEE Access
Multidisciplinary | Rapid Review | Open Access Journal

Received 28 March 2024, accepted 14 April 2024, date of publication 22 April 2024, date of current version 30 April 2024.

Digital Object Identifier 10.1109/ACCESS.2024.3392477

RESEARCH ARTICLE

Performance of Spatially Coupled LDPC Codes Over the Underwater Wireless Optical Channel With Strong Turbulence and Pointing Errors

SRAVAN KUMAR PADALA AND JOHN D'SOUZA, (Member, IEEE)
Department of Electronics and Communication Engineering, National Institute of Technology Karnataka, Surathkal, Karnataka 575025, India
Corresponding author: Sravan Kumar Padala (sravan.ec16f12@nitk.edu.in)

This work was supported by the National Institute of Technology Karnataka under the MoU with IEEE open access policy.

ABSTRACT The major problems in an underwater wireless optical communication (UWOC) link are turbulence induced fading and pointing errors. In this paper, we have investigated the bit error rate (BER) performance of spatially coupled low-density parity-check (SC-LDPC) coded horizontal UWOC link over a strong turbulent channel model with pointing errors. The performance of this link for different channel and code parameters has been studied using simulations. It has been observed that a rate 1/2 ARJA protograph based SC-LDPC code with graph lifting factor of 256 gives a coding gain of 47 dB at a BER of 10^{-4} for strong turbulence channel model with pointing errors. An analytical BER expression for an uncoded UWOC link under strong turbulence with pointing errors for the On-Off Keying modulation technique has been derived. A multidimensional protograph based extrinsic information transfer algorithm has been developed to obtain the decoding thresholds for different channel parameters and code rates. We have also studied the SC-LDPC coded vertical UWOC link performance for some specific strong turbulence channel parameters with pointing errors and observed that as the link length increases from 20 *m* to 40 *m*, the performance gap between the hypothetical and cascaded channel models increases from 1.1 *dB* to 5.5 *dB*.

INDEX TERMS Bit error rate, low-density parity-check codes, pointing errors, protograph, scintillation index, spatially coupled LDPC codes, underwater optical wireless communication.

I. INTRODUCTION

Underwater wireless optical communication (UWOC) [1], [2] is a high bandwidth, low-cost deploy-ability system. There is a lot of interest in UWOC because of its applications in the internet of underwater things (IoUT) [3], [4], underwater wireless sensor networks (UWSN) [5], oil, gas and mineral exploration, navigation, military etc. The major impairment in a UWOC link is underwater turbulence [6], [7] which causes irradiance fluctuations. The strength of turbulence depends on the temperature and salinity fluctuations. In [8] and [9], an experimental investigation has been conducted on the statistical distribution of underwater fading and the log-normal and Gamma-Gamma (GG) probability density functions (PDFs) have been found to match the experimental results for weak and moderate/strong turbulence conditions respectively. Typically strong turbulence occurs for large link lengths, but it can also occur at short distances depending on the dissipation rate of the mean-square temperature. The case of strong turbulence arises in applications like IoUT, UWSN, autonomous underwater vehicles (AUV) and remotely operated underwater vehicles (ROV) etc. If the transmitter and receiver are not aligned properly, the system introduces pointing errors [10]. In the literature, the beam spread function [11] and the geometric loss model [12], [13] have been used to study the effect of the pointing errors on the signal strength. The pointing errors and the irradiance fluctuations deteriorate the UWOC system performance. The

The associate editor coordinating the review of this manuscript and approving it for publication was Yogendra Kumar Prajapati.

error correcting codes can be used to improve the system's performance.

In [14] and [15], a Reed-Solomon channel coded system has been studied for reliable operation of UWOC links using only the path loss model. The LDPC coded and BCH coded weak turbulent UWOC systems have been studied in [16] and [17] respectively using the log-normal distribution model. The uncoded strong turbulent channel model has been studied in [6], [18], [19], and [20] using GG distribution model. Different strong turbulent channel models have been studied in [8] and [9] through experimental results. However, a channel coded strong turbulent UWOC system has not been investigated in literature. Furthermore, although pointing errors are always present in an optical link, only a few authors have studied UWOC turbulent system with pointing errors [12], [13], [21]. In this paper, we have investigated the bit error rate (BER) performance of a spatially coupled low-density parity-check (SC-LDPC) coded strong turbulent channel with pointing errors.

The LDPC codes are a class of capacity achieving block codes whose complexity grows linearly with block length. The SC-LDPC codes [22] are a sub class of LDPC codes, which have the combined positive features of linear minimum distance growth (like the regular LDPC codes) and better decoding threshold (like the irregular LDPC codes). The decoding threshold divides the channel parameter (signal to noise ratio (SNR) or noise variance or erasure probability) space into two regions. In one region low bit error rates, that is reliable communication can be achieved whereas in the other region, low bit error rates are not possible. In this paper, minimum transmitted power required to achieve the low error probability is considered as decoding threshold. In the literature, the decoding threshold of LDPC codes has been obtained using density evolution (DE) [23] and extrinsic information transfer (EXIT) chart analysis [24]. The SC-LDPC codes have been shown to achieve convolutional gains compared to underlying LDPC block codes over the additive white Gaussian noise (AWGN) channel [25]. These codes have been studied over the underwater acoustic communication channel in [26] and were found to give improvement in performance compared to the LDPC codes. In this paper, we have studied the performance of a protograph [27] based SC-LDPC coded UWOC link for different turbulence strengths and pointing errors. Different code rates and encoder and decoder parameters have been considered in order to study the effect of these parameters on the UWOC link performance. The decoding thresholds have also been obtained by modifying the classical protograph based extrinsic-information-transfer (P-EXIT) algorithm [28], for different channel parameters and code rates. Although our study is focused on the horizontal link, we have also studied the SC-LDPC coded vertical UWOC link [29] performance for some specific strong turbulence channel parameters.

The contributions made in this paper are as follows.

1) The performance of a UWOC system has been studied over a strong turbulence channel with pointing errors using SC-LDPC codes for different code rates, encoding and decoding parameters, turbulence strengths and pointing errors.
2) A closed-form expression quantifying the analytical BER for On-Off Keying (OOK) modulated uncoded UWOC system over a GG channel with pointing errors has been derived.
3) A multidimensional modified P-EXIT algorithm has been developed to obtain the decoding thresholds for various channel parameters and code rates. Our approach is applicable to the memoryless binary-input symmetric-output channels.
4) The SC-LDPC coded vertical UWOC link has been studied for the cascaded channel model.

The rest of the paper is organized as follows. The system and channel models are briefly described in Section II. The construction, encoding and decoding of SC-LDPC codes are outlined in Section III. The derivation of analytical BER expression, BER calculation using kernel-based density estimation and multi dimensional P-EXIT algorithm are described in Section IV. The simulation results are discussed in Section V and is followed by conclusions in Section VI.

II. SYSTEM MODEL

The SC-LDPC coded UWOC system is used for point to point communication. The encoded data is modulated with OOK and transmitted through the channel. The signal z at the receiver is given by [30],

$$z = r_p I R \sqrt{P_t T_b} x + n \tag{1}$$

where $x \in \{0, 1\}$ is transmitted data, I is channel fading coefficient, $r_p = 0.15\ A/W$ is receiver responsivity, R is code rate, P_t is transmitted power, T_b is bit duration and n is AWGN with mean zero and variance σ^2. The dominant source of noise in the UWOC system is thermal noise. This noise has been modeled as Gaussian distribution with mean zero and variance $\sigma^2 = (4K_B T_e B_e)/R_L$, where $K_B = 1.38 \times 10^{-23}\ J/K$ is Boltzmann constant, $T_e = 256\ K$ is absolute receiver temperature, $B_e = 2/T_b$ is electronic bandwidth and $R_L = 100\ \Omega$ is load resistance [17], [31]. The channel model considered in (1) is a combination of turbulence and pointing errors, and the overall channel fading coefficient can be represented [19] and [30] as

$$I = I_t I_p \tag{2}$$

where I_t is random attenuation due to turbulence and I_p is fading coefficient due to geometric spread and pointing errors. The parameters I_t and I_p are discussed further in Sections II-A and II-B.

A. TURBULENCE CHANNEL MODEL

As the physical mechanism of underwater optical turbulence is similar to that of atmospheric optical turbulence, the theory

of atmospheric turbulence has been applied to underwater optical turbulence [32]. The channel turbulence can be categorized into weak, moderate and strong turbulence [6]. The weak turbulence has been modeled as log-normal distribution [16], [33], [34], whereas moderate and strong turbulence have been modeled as GG distribution [6], [10], [29]. In [8] and [9], from the experimental results it was observed that for strong turbulence the GG model is a better fit with the experimental data. Other authors [18], [20], and [29] have also used the GG channel model for the UWOC system under strong turbulence. The density function of the GG distribution is given as

$$f_{I_t}(I_t) = \frac{2(\alpha\beta)^{\frac{\alpha+\beta}{2}}}{\Gamma(\alpha)\Gamma(\beta)} I_t^{\frac{\alpha+\beta}{2}-1} K_{\alpha-\beta}\left(2\sqrt{\alpha\beta I_t}\right), \; I_t \geq 0 \quad (3)$$

where $K_m(\cdot)$ is m^{th} order modified Bessel function of the second kind and $\Gamma(\cdot)$ is the Gamma function, α and β represent large and small scale turbulent eddies. These α and β values can be calculated [29] with the assumption of plane wave propagation using the expressions

$$\alpha = \left[exp\left(\frac{0.49\sigma_I^2}{\left(1 + 1.11\sigma_I^{12/5}\right)^{7/6}} \right) - 1 \right]^{-1}, \quad (4)$$

$$\beta = \left[exp\left(\frac{0.51\sigma_I^2}{\left(1 + 0.69\sigma_I^{12/5}\right)^{5/6}} \right) - 1 \right]^{-1}, \quad (5)$$

where σ_I^2 is termed scintillation index (SI). σ_I^2 has been used to indicate the strength of turbulence. The value of σ_I^2 depends on the power spectrum model being used for turbulent fluctuations. Even though (4) and (5) are commonly used for free space optical (FSO) links in literature, the power spectrum model used in these equations is different for UWOC links and FSO links. In order to determine σ_I^2, the spatial power spectrum of turbulent fluctuations for sea water refractive index has been used [35], [36] and is given by

$$\Phi_n(\kappa) = 0.388 \times 10^{-8} \varepsilon^{-1/3} \kappa^{-11/3} [1 + 2.35(\kappa\eta)^{2/3}] \times \frac{\chi_T}{\omega^2} \left(\omega^2 e^{-A_T\delta} + d_r e^{-A_S\delta} - \omega(d_r + 1) e^{-A_{TS}\delta} \right) \quad (6)$$

where d_r is eddy diffusivity ratio, ω is relative strength of temperature and salinity fluctuations, η is Kolmogorov micro-scale, χ_T is the rate of dissipation of mean-square temperature, $\delta = 8.284(\kappa\eta)^{4/3} + 12.978(\kappa\eta)^2$, and $A_S = 1.9 \times 10^{-4}, A_T = 0.01863, A_{TS} = 9.41 \times 10^{-3}$. Even though eddy diffusivities of temperature and salt are different, many of the previous studies of UWOC links assumed $d_r = 1$ [35], [37]. The relation between the value of d_r and ω is given in [36]. After obtaining the $\Phi_n(\kappa)$ value, the σ_I^2 value can be calculated by using the expression [29], [35]

$$\sigma_I^2 = 8\pi^2 k_0^2 d_0 \int_0^1 \int_0^\infty \kappa \Phi_n(\kappa) \left(1 - cos\left(\frac{\kappa^2 d_0}{k_0}\zeta\right)\right) d\kappa d\zeta, \quad (7)$$

where $k_0 = \frac{2\pi}{\lambda}$, λ is wavelength and d_0 is link length.

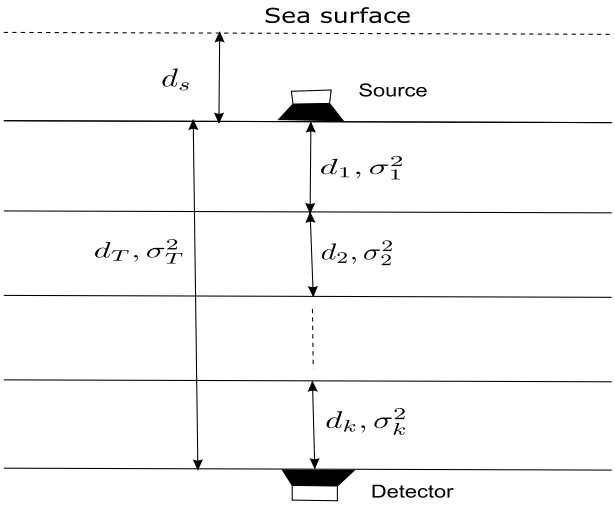

FIGURE 1. Vertical underwater link with different layers.

In the UWOC horizontal links, the turbulence strength is usually considered as constant throughout the link length (transmission range). This is not the case with the vertical links, where the source and destination are located at different depths in underwater. Since the temperature and the salinity vary with depth of the water, the turbulence strength also varies accordingly. This leads to the stratification of underwater environment. In [29], the vertical underwater link has been modeled as a collection of successive layers with different lengths as shown in Fig. 1, where the source is located at depth d_s from the sea surface and the j^{th} layer has a thickness of $d_j, j = 1, 2, .., k$. Here the fading coefficient of each layer has been treated as independent and modeled as a GG random variable with a different SI value. Therefore the overall fading coefficient (I_{vt}) can be obtained by multiplying the fading coefficients of various layers and is given by

$$I_{vt} = \prod_{j=1}^{k} I_j \quad (8)$$

where I_j is the j^{th} layer fading coefficient and follows the GG distribution with SI value σ_j^2.

B. POINTING ERRORS

The line of sight underwater optical link performance depends on the link pointing precision. However, the waves and the ocean currents result in the movements of the optical source and detector. In the literature [11], [12], [13], two approaches have been adopted to account for the effect of pointing errors on the signal strength in an UWOC system.

In the first approach [11] the beam spread function has been used to measure the optical power received at the receiver as a function of deviation of the receiver from the main beam axis and link length. In the second approach [12], [13], the misalignment effect has been considered by assuming the random radial displacement of the beam spot from the line of sight (LOS) position. The actual channel model should include the multipath effect and the resulting delay spread and inter symbol interference (ISI). However, UWOC is not much affected by this effect because of the high speed and short distance communication links [5], [38], [39]. We have considered the second approach in our study, since it has been widely used and is easier to analyze in different channel conditions. In this approach the pointing errors and their effect can be represented by fading coefficient as

$$I_p \approx A_0 e^{-2s^2/\Omega_{zeq}^2} \tag{9}$$

where $A_0 = (\text{erf}(\vartheta))^2$ is path loss constant, $\Omega_{z_{eq}} = \Omega_z\sqrt{\sqrt{\pi}\,\text{erf}(v)/(2v \times exp(-v^2))}$ is equivalent beam radius at receiver, $\vartheta = \left(\sqrt{\pi}r\right) / \left(\Omega_z\sqrt{2}\right)$, Ω_z is beam waist and r is the radius of the detector. The PDF of the displacement of the beam at the detector has a Rayleigh distribution with variance σ_s^2, when the radial displacement of the beam, in both the vertical and horizontal directions, is treated as an independent identically distributed Gaussian random variable. This displacement PDF can be written as

$$f_s(s) = \frac{s}{\sigma_s^2} e^{-s^2/2\sigma_s^2}. \tag{10}$$

By using (9) and (10) the PDF of I_p for a circular detector can be expressed [30] and [40] as

$$f_{I_p}(I_p) = \frac{\xi^2}{A_0^{\xi^2}} I_p^{\xi^2-1}, \quad 0 \le I_p \le A_0 \tag{11}$$

where $\xi = \frac{\Omega_{zeq}}{2\sigma_s}$ and σ_s is the standard deviation of pointing error displacement at the receiver.

C. COMBINED CHANNEL

The PDF of the overall channel coefficient ($I = I_l I_p$) is given as [19]

$$f_I(I) = \frac{\alpha\beta\xi^2}{A_o\Gamma(\alpha)\Gamma(\beta)} G_{1,3}^{3,0}\left(\frac{\alpha\beta I}{A_o}\middle|\begin{matrix}\xi^2\\ \xi^2-1,\alpha-1,\beta-1\end{matrix}\right), \tag{12}$$

where $G_{m,n}^{p,q}[\cdot]$ is the Meijer G-function.

III. SPATIALLY COUPLED LDPC CODES

We have used SC-LDPC codes to improve the UWOC system performance. In this section, we briefly describe the LDPC codes in III-A, the construction of SC-LDPC codes in III-B and the decoding of SC-LDPC codes in III-C.

A. LDPC CODES

A (J, K)- regular LDPC block code (LDPC-BC) can be represented by a sparse parity check matrix H, which contains exactly J number of ones in every column and K number of ones in every row. If the row and column weights vary, the LDPC-BC is said to be irregular. The matrix H can be represented using a bipartite graph called Tanner graph, where in, the columns and rows of H correspond to variable nodes and check nodes of the Tanner graph respectively. An edge is connected between check node i and variable node j if the position (i, j) of matrix H contains 1.

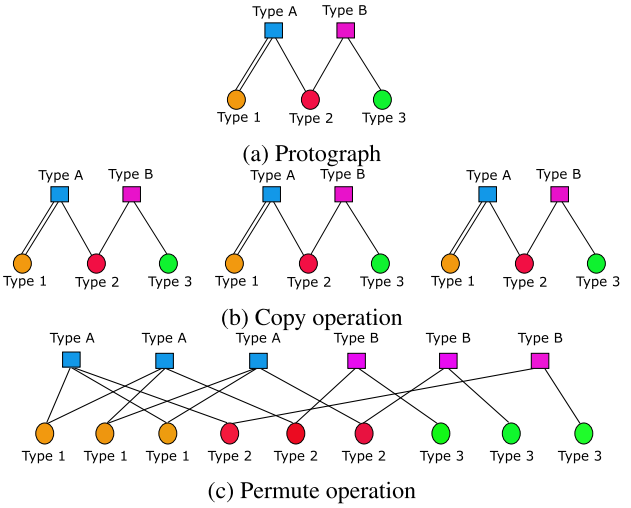

FIGURE 2. Protograph with graph lifting factor M = 3: (a) protograph with 2 check nodes and 3 variable nodes, (b) copy operation (c) Permutation operation.

We have used the protograph based method [27] to obtain the parity check matrix. A protograph is a small Tanner graph with few nodes and edges and it can be represented by its bi-adjacency matrix B. The element $b_{i,j}$ of B represents the number of edges connected between i^{th} check node and j^{th} variable node. In general, a protograph can have more than one edge between a variable node and a check node, which means $b_{i,j}$ can be greater than 1. An example of a protograph is shown in Fig. 2a. This protograph can be represented by its bi-adjacency matrix as

$$B = \begin{bmatrix} 2 & 1 & 0 \\ 0 & 1 & 1 \end{bmatrix}.$$

From this protograph, a larger Tanner graph can be obtained by using copy and permute operations as shown in Fig. 2b and Fig. 2c respectively. In this operation, first M copies of protograph are generated. The edges connected to a particular check node are permuted among the M variable nodes of the same type to which they were connected originally. This process is called graph lifting and the number of copies (M) used in the process is called lifting factor. In the graph lifting procedure each non-zero entry in B is replaced by sum of $b_{i,j}$ number of $M \times M$ permutation matrices and each 0 in B is replaced by $M \times M$ zero matrix, where the permutation matrix consists exactly one entry of 1 in each row and column and 0 elsewhere. Then the H matrix corresponding to the large

tanner graph can be written as

$$H = \left[\begin{array}{ccc|ccc|ccc} 1 & 0 & 1 & 1 & 0 & 0 & 0 & 0 & 0 \\ 1 & 1 & 0 & 0 & 1 & 0 & 0 & 0 & 0 \\ 0 & 1 & 1 & 0 & 0 & 1 & 0 & 0 & 0 \\ \hline 0 & 0 & 0 & 0 & 1 & 0 & 1 & 0 & 0 \\ 0 & 0 & 0 & 0 & 0 & 1 & 0 & 1 & 0 \\ 0 & 0 & 0 & 1 & 0 & 0 & 0 & 0 & 1 \end{array}\right].$$

This process preserves the degree distribution, rate and computation graph of the protograph.

B. SC-LDPC CODES CONSTRUCTION

The SC-LDPC codes can be obtained by coupling a sequence of LDPC block codes as follows [22]. Let the LDPC block code be represented by a protograph with base matrix B. L copies of the protographs are taken and the protographs are interconnected by a process called edge spreading as shown in Fig. 3. In this process, the edges associated with the variable node at time t are connected to the check nodes at time $t+i$, $i = 0,1,..w$. The edge spreading rule must satisfy the condition

$$\sum_{i=0}^{w} B_i = B_{b_c \times b_v} \tag{13}$$

where B_i are component base matrices, b_c and b_v are number of rows and columns of base matrix B and w is memory or coupling width of the SC-LDPC code. The edge spreading operation is depicted in Fig. 3 for a regular-(3,6) LDPC block code with $w = 2$, $B = \begin{bmatrix} 3 & 3 \end{bmatrix}$ and $B_0 = \begin{bmatrix} 1 & 1 \end{bmatrix} = B_1 = B_2$. The resulting SC-LDPC code base protograph with coupling length $L = 5$ is shown in Fig. 3b. This SC-LDPC protograph can be represented in matrix form as

$$B_{[0,L-1]} = \begin{bmatrix} B_0 & & & & \\ B_1 & B_0 & & & \\ B_2 & B_1 & B_0 & & \\ & B_2 & B_1 & B_0 & \\ & & B_2 & B_1 & B_0 \\ & & & B_2 & B_1 \\ & & & & B_2 \end{bmatrix}_{(L+w)b_c \times Lb_v}.$$

After obtaining the SC-LDPC base protograph, the extended parity check matrix can be obtained by applying the graph lifting procedure to this protograph.

Carefully designed protograph based SC-LDPC codes can achieve better thresholds and linear minimum distance growth. One such protograph is accumulate-repeat-jagged-accumulate (ARJA) [41] and is shown in Fig. 4a. In Fig. 4, variable nodes are numbered as 0,1,2,3,4 and check nodes are numbered as 0,1,2. The punctured variable nodes in these protographs are represented by white circles. The lifted graph has the punctured variable nodes increased by a factor of M. The protograph in Fig. 4a can also be represented as shown in Fig. 5a. The base matrix of the ARJA protograph with design rate $1/2$ is

$$\underset{b_c \times b_v}{B} = \begin{bmatrix} 1 & 2 & 0 & 0 & 0 \\ 0 & 3 & 1 & 1 & 1 \\ 0 & 1 & 2 & 1 & 2 \end{bmatrix},$$

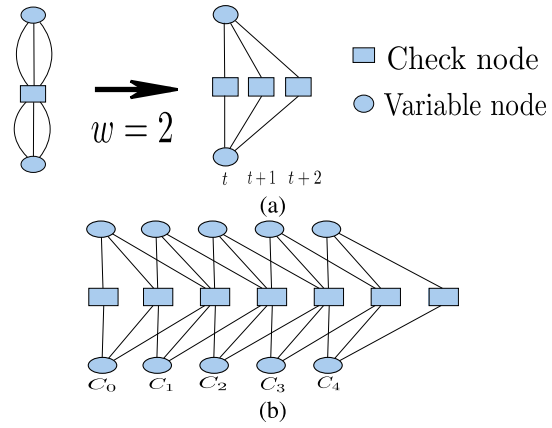

FIGURE 3. (a) Edge spreading of (3,6)-regular LDPC block code protograph with $w = 2$, (b) Protograph of SC-LDPC code with $L = 5$.

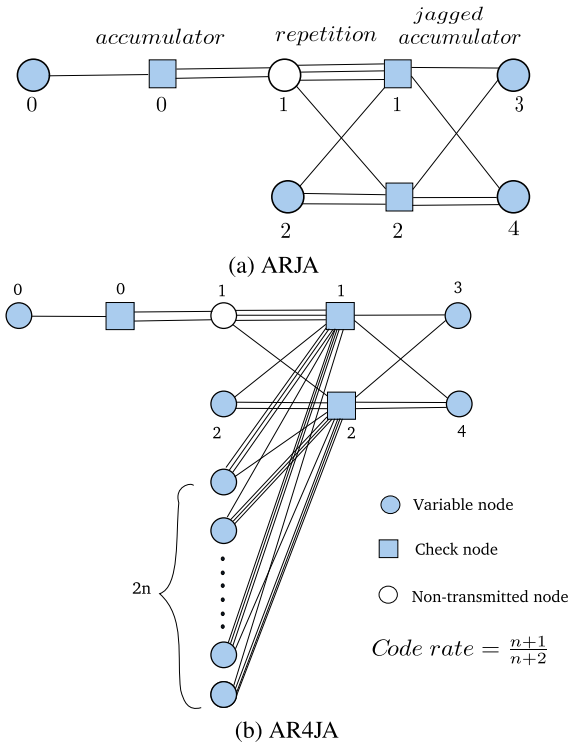

FIGURE 4. Protographs of irregular LDPC block code ensemble: (a) ARJA protograph with rate = 1/2, (b) AR4JA protograph with rate = (n+1)/(n+2).

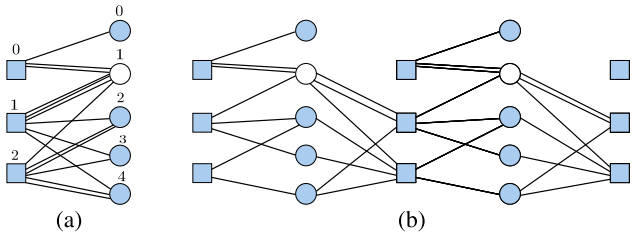

FIGURE 5. (a) ARJA protograph (b)ARJA based SC-LDPC protograph with $w = 1$ and $L = 2$.

where b_c and b_v are the number of check nodes (rows) and variable nodes (columns) of protograph (base matrix)

respectively. Different code rates can be obtained by adding extra variable nodes to ARJA protograph as shown in the Fig. 4b, the resulting protograph is called as accumulate-repeat-by-4-jagged-accumulate (AR4JA). In [22], the SC-LDPC codes have been constructed by using ARJA and AR4JA protographs with $w = 1$, $L = 10$ and are denoted as $C_A(n)$, where $2n$ is extra variable nodes added to the ARJA protograph. The component base matrices obtained according to the edge spreading rule are

$$B_{0\ b_c \times b_v} = \begin{bmatrix} 1 & 2 & 0 & 0 & 0 \\ 0 & 1 & 1 & 1 & 0 \\ 0 & 0 & 1 & 0 & 1 \end{bmatrix},$$

$$B_{1\ b_c \times b_v} = \begin{bmatrix} 0 & 0 & 0 & 0 & 0 \\ 0 & 2 & 0 & 0 & 1 \\ 0 & 1 & 1 & 1 & 1 \end{bmatrix},$$

where $\sum_{i=0}^{w} B_i = B$. These component base matrices have been used to obtain the protograph of SC-LDPC code and is shown in Fig. 5b for the case of $w = 1$ and $L = 2$. Now the graph lifting procedure is applied for the protograph of SC-LDPC code to obtain the larger Tanner graph (parity-check matrix).

In conventional approach, the graph lifting procedure has been carried out using the permutation matrices [27]. In our study, we have used the progressive edge growth (PEG) algorithm [42] in the graph lifting procedure, since this algorithm eliminates the short cycles in the Tanner graph. The resulting parity check matrix is used in encoding the data. In the literature, different encoding methods are available for the class of LDPC codes [43], [44]. We have used the partial syndrome former method [44] to encode SC-LDPC codes, since this method uses the structure of SC-LDPC codes to reduce computational complexity and memory requirement. In the following, the PEG algorithm and the partial syndrome former encoding method are briefly described.

1) PEG ALGORITHM

The PEG algorithm generates the Tanner graph, given the number of variable nodes, check nodes and degree distribution of variable nodes. This algorithm works by adding one edge at a time to the graph in such a way that local girth of the graph is maximized. This algorithm is a greedy algorithm for generating the Tanner graph. Let us assume that there is a code with n variable nodes and m check nodes. For each variable node j, let d_j be the degree of variable node j and let $D_v = \{d_0, d_1, d_2, \ldots, d_{(n-1)}\}$ be the degree distribution sequence of the variable nodes. The set of check nodes reachable from variable node j within depth l is denoted by N_j^l and the set of check nodes not present in N_j^l is denoted by $\bar{N}_j^l$. A Tanner graph can be represented by a set of edges $E = E_1 \cup E_2 \cup \ldots \cup E_n$, where E_j is a set of edges incident on variable node j. In the case of protograph based codes, the check node selection is based on the type of variable node and check node connection in the original protograph. Consider an example of a protograph shown in Fig. 2a. Let the graph

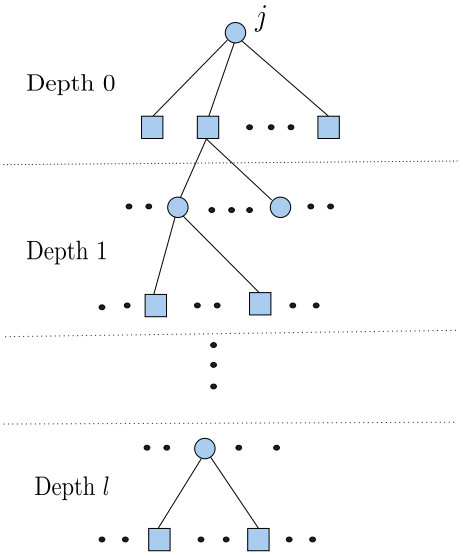

FIGURE 6. Expansion of graph from the variable node j up to the depth l.

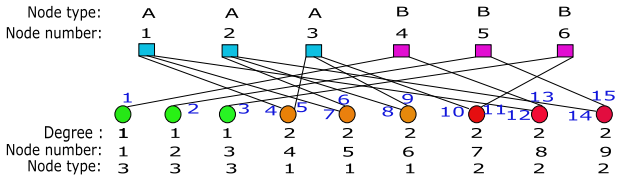

FIGURE 7. Tanner graph generated using PEG algorithm. Edges are numbered (in blue colour) according to the order of their connection to the Tanner graph.

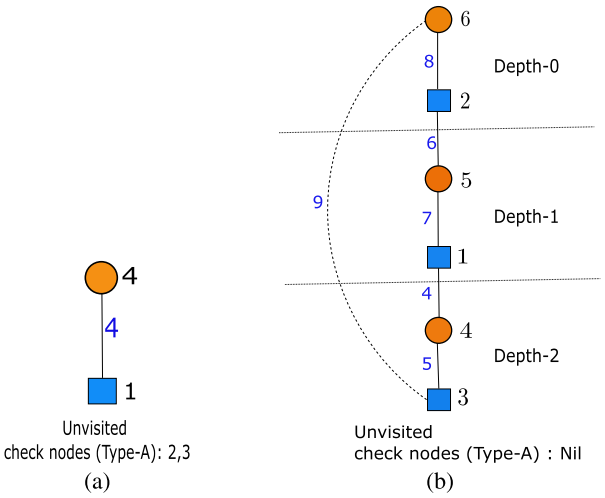

FIGURE 8. Expansion of subgraph from (a) variable node 4 (b) variable node 6.

lifting factor be $M = 3$. After the copy operation, the PEG algorithm operates as follows.

(i) Initialization: The variable nodes are arranged according to their degrees in ascending order as shown in Fig. 7. Degrees of all the check nodes are initialized with zero value. Thus to start with, the subgraph consists of only the variable nodes and check nodes and no edges. Then, one variable node

is selected at a time in the order of ascending degree and edges are connected to it by following the next two steps.

(ii) For the selected variable node, the first edge is connected with the check node having the minimum degree under the current subgraph. In our example, the variable node 1 is connected to check node 4, by randomly selecting one among the check nodes 4, 5 and 6, since these check nodes are of type-B and have the degree 0 under current subgraph. After connecting edge-1, the degree of check node 4 increases by 1. Next the algorithm selects the variable node 2 and an edge is connected to it, by selecting the check node 5 (randomly among the available check nodes 5 and 6). Similarly, the single edge of variable node 3 and the first edge of variable node 4 are connected to check nodes 6 and 1 respectively.

(iii) For a connection of an edge, other than the first edge of a selected variable node j, a check node is selected in such a way that the local girth is maximized. To achieve this, a subgraph is expanded from variable node j as shown in Fig. 6 and a check node is selected from the set of check nodes that are not visited ($\bar{N}_j^l$) by the expanded subgraph. From the set $\bar{N}_j^l$, a check node with minimum degree is selected and an edge is placed between the variable node j and this check node. This case arises in our example for the connection of the second edge at the variable node 4 (edge-5). The expanded subgraph from the variable node 4 is shown in Fig. 8a. It is observed that the check nodes 2 and 3 are not visited by the expanded subgraph. Therefore the variable node 4 is connected to check node 3 (chosen randomly among the check nodes 2 and 3) and the degree of check node 3 is increased by 1. Similarly, the two edges of variable node 5 and first edge of variable node 6 can be connected using steps (ii) and (iii).

The case of set $\bar{N}_j^l = \phi$ arises when the expanded subgraph of a variable node j has all the check nodes visited within depth l. In that case a check node of minimum degree is selected from the set of check nodes that are at depth l. This results in a graph that has a cycle with length $2(l+1)$. Thus this algorithm maximizes the local girth. In our example this case arises for the connection of second edge of variable node 6 (edge-9). The expanded subgraph from variable node 6 is shown in Fig. 8b. It is observed that all the check nodes are visited in the expanded subgraph at depth-2. Therefore the check node at depth-2 (check node 3) is selected and an edge is placed (edge-9).

(iv) This procedure continues until the edges are connected to all the variable nodes according to their degree distribution. At the end of the algorithm the Tanner graph shown in Fig. 7 is generated.

2) PARTIAL SYNDROME FORMER

The partial syndrome former method gives the parity part of the systematic SC-LDPC code. This partial syndrome former encoder realization of LDPC convolutional codes is proposed and analyzed in [44] and is described in the following. Consider a transposed parity check matrix (syndrome former) of the convolutional code as shown in (14), at the bottom of the next page. Let binary LDPC convolutional code rate be $R = \frac{b}{c}$. The sub matrices $H_i(t)$, $i = 0, 1, ..w$, are binary sub matrices of size $(c-b) \times c$ and satisfy the following properties:

1) $H_i(t) = 0$, $i < 0$ and $i > w$, $\forall t$
2) There is a t such that $H_w(t) \neq 0$
3) $H_0(t) \neq 0$, $\forall t$, has full rank.

Here w is called the syndrome former memory and the width of diagonal structure of syndrome former (constraint length) is $(w+1)c$. Let $v_{[0,t-1]} = [v_0, v_1, .., v_{t-1}]$ be the sequence of systematically encoded code symbols corresponding to a block of information symbols $u_{[0,t-1]} = [u_0, u_1, .., u_{t-1}]$, where $v_k = (v_k^{(1)}, v_k^{(2)}, .., v_k^{(c)})$, $u_k = (u_k^{(1)}, u_k^{(2)}, .., u_k^{(b)})$, $k = 0, 1, .., t-1$. A code sequence satisfies the condition

$$v_{[0,t-1]} H_{[0,t-1]}^T = [0_{[0,t-1]} | p_t] \tag{15}$$

where $0_{[0,t-1]}$ is vector with zeros as elements, $p_t = [p_{t,1}, p_{t,2}, .., p_{t,w}]$ and $p_{t,i} = (p_{t,i}^{(1)}, p_{t,i}^{(2)}, .., p_{t,i}^{(c-b)})$, $i = 1, 2, .., w$. Here p_t is called as the partial syndrome. From (15), p_t can be calculated recursively as a function of v_{t-1} and p_{t-1} using

$$p_{t,i} = \begin{cases} p_{t-1,i+1} + v_{t-1} H_i^T(t+i-1), & i = 1, 2, ..w-1 \\ v_{t-1} H_w^T(t+w-1), & i = w. \end{cases} \tag{16}$$

We assume a systematic encoder and let $v_k = [v_{k,0}, v_{k,1}]$, where $v_{k,0}$ is information sequence u_k and $v_{k,1}$ is parity check vector. The parity bits can be generated at time t given the encoder state, using

$$[v_{t,0}, v_{t,1}] H_0^T(t) = p_{t,1} \tag{17}$$

Let $H_0(t) = [H_0^{(0)}(t), H_0^{(1)}(t)]$, where $H_0^{(0)}(t)$ is $(c-b) \times b$ matrix and $H_0^{(1)}(t)$ is $(c-b) \times (c-b)$ full rank matrix. Then from (17)

$$v_{t,0} [H_0^{(0)}(t)]^T + v_{t,1} [H_0^{(1)}(t)]^T = p_{t,1}. \tag{18}$$

If $H_0^{(1)}(t)$ is an identity matrix then $v_{t,1} = v_{t,0} [H_0^{(0)}(t)]^T + p_{t,1}$. This gives the parity part of the code.

Now to encode the terminated LDPC convolutional code (SC-LDPC code), the tail bits must be added to force the encoder to the zero state. Consider SC-LDPC code with coupling length L and information sequence $u_{[0,L-1]}$. Then the tail $v_{[L,L+\tau-1]}$ of $c\tau$ symbols must be determined corresponding to $u_{[L,L+\tau-1]}$ to force the encoder to zero state. This means

$$v_{[0,L+\tau-1]} H_{[0,L+\tau-1]}^T = 0_{[0,L+\tau+w-1]} \tag{19}$$

Now (19) can be split in to two equations

$$v_{[0,L-1]} H_{[0,L-1]}^T = \left[0_{[0,L-1]} | p_L\right] \tag{20}$$

and

$$v_{[L,L+\tau-1]} H_{[L,L+\tau-1]}^T = \left[p_L | 0_{[0,\tau-w-1]}\right]. \tag{21}$$

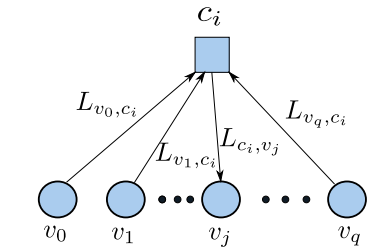

(a) Check node c_i to variable node v_j LLR

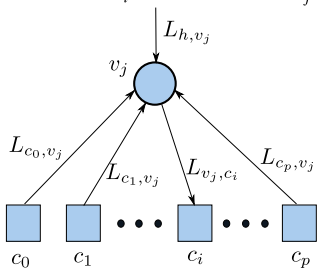

(b) Variable node v_j to check node c_i LLR

FIGURE 9. Message passing algorithm.

In (21) some of the equations are linearly dependent. If all dependent columns of $H^T_{[L,L+\tau-1]}$ are removed, then we obtained the $c\tau \times \psi$ matrix $F(L)$. Now (21) becomes

$$v_{[L,L+\tau-1]}F(L) = [p^*_L|0], \tag{22}$$

where p^*_L is obtained after removing the redundant components from p_L and $\mathbf{0}$ is a zero vector. The length of $[p^*_L|0]$ is ψ. $F(L)$ is full rank matrix and will have a pseudo inverse. From (22)

$$v_{[L,L+\tau-1]} = [p^*_L|0]F^{-1}(L). \tag{23}$$

By using the above equation the termination tail can be determined.

For a (J,K) regular protograph, the encoding complexity per bit of this syndrome former method is proportional to (K-1) and the memory requirement for the encoder realization is (c-b)(w+1)M [44].

C. DECODING

The belief propagation (BP) algorithm [45] is used for decoding the class of LDPC codes. In this algorithm, during each iteration, log-likelihood ratio (LLR) values will be passed from variable node to check node (L_{v_j,c_i}) and check node to variable node (L_{c_i,v_j}) as shown in Fig. 9. These LLRs

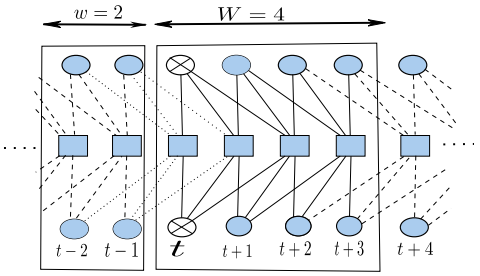

FIGURE 10. Sliding window at decoding position t with window length $W = 4$ and memory of the SC-LDPC code $w = 2$.

can be calculated as follows [46]

$$L_{v_j,c_i} = L_{h,v_j} + \sum_{l\in N(v_j)\setminus i} L_{c_l,v_j} \tag{24}$$

$$L_{c_i,v_j} = 2\tanh^{-1}\left(\prod_{l\in N(c_i)\setminus j}\tanh\left(\frac{L_{v_l,c_i}}{2}\right)\right) \tag{25}$$

where L_{h,v_j} is LLR from channel to variable node j, $N\left(v_j\right)\setminus i$ is a set of check nodes connected to variable node j excluding check node i. Similarly, $N\left(c_i\right)\setminus j$ is a set of variable nodes connected to check node i excluding variable node j. At the end of each iteration, for each variable node, output LLR is calculated as

$$L_{out,v_j} = L_{h,v_j} + \sum_{l\in N(v_j)} L_{c_l,v_j} \tag{26}$$

The iterative process will continue until all the symbols are decoded or a preset maximum number of iterations is reached.

The SC-LDPC codes can be decoded by applying the BP algorithm to the entire block of L coupled LDPC block codes. This approach results in increased complexity with the increase in L. The structure of SC-LDPC codes is useful in applying the windowed decoding approach [47], [48] and results in lower complexity and reduced decoding latency. The sliding window decoding approach has been used in this paper. In this method, the size of window W should be greater than the memory w of the SC-LDPC code. The complexity of this decoding approach depends on W but is independent of L for a given value of M.

An example of a sliding window decoding approach is shown in Fig. 10: the window size is $W = 4$ and the edges are spread as shown in Fig. 3. At each decoding window position t, only the variable nodes at location t, called target nodes are decoded. After the target nodes are decoded or a

$$H^T_{[t,t']} = \begin{bmatrix} H^T_0(t) & \cdots & \cdots & H^T_w(t+w) & 0 & & \\ 0 & H^T_0(t+1) & \cdots & & H^T_w(t+w+1) & \ddots & \\ \vdots & 0 & \ddots & \vdots & \vdots & \ddots & 0 \\ \vdots & \vdots & \ddots & H^T_0(t') & \cdots & & H^T_w(t'+w) \end{bmatrix}, \quad t \le t' \tag{14}$$

preset maximum number of iterations is reached, the window slides to the next decoding position (i.e. $t+1$). This process continues until all the variable nodes are decoded.

The decoding latency of SC-LDPC codes under the sliding window decoding algorithm is WbM information bits; and the processor design complexity is $(w+1)cM$ [44].

IV. PERFORMANCE ANALYSIS

In this section, the derivation of analytical BER expression for the uncoded UWOC system over GG channel with pointing errors is given in IV-A; the BER calculation using kernel-based density estimation is described in IV-B and P-EXIT algorithm to obtain the decoding threshold is described in IV-C.

A. ANALYTICAL BER EVALUATION

The BER associated with the OOK modulated uncoded UWOC system under the influence of strong turbulence without pointing errors, assuming GG channel is given as [49]

$$P_e = \frac{2^{\alpha+\beta-1}}{2\pi\Gamma(\alpha)\Gamma(\beta)} \times \sum_{i=1}^{2}\left(D_i G_{4,1}^{1,4}\left(\begin{matrix}\frac{1-\alpha}{2},\frac{2-\alpha}{2},\frac{1-\beta}{2},\frac{2-\beta}{2}\\ 0\end{matrix}\middle| A_i\left(\frac{\eta\sqrt{\frac{P_t T_b}{\sigma^2}}}{\alpha\beta}\right)^2\right)\right), \tag{27}$$

where $D_1 = \frac{1}{12}$, $D_2 = \frac{1}{4}$, $A_1 = 2$ and $A_2 = \frac{8}{3}$. By considering both turbulence and pointing errors and assuming the GG channel model, the BER can be calculated using [50],

$$P_e = \int_0^\infty f_I(I)\mathbb{Q}\left(\eta I\sqrt{\frac{P_t T_b}{4\sigma^2}}\right)dI \tag{28}$$

where $\mathbb{Q}(x) \triangleq \frac{1}{\sqrt{2\pi}}\int_x^\infty \exp\left(-\frac{y^2}{2}\right)dy$ is Q-function. The Q-function can be approximated [51] as $\mathbb{Q}(x) \approxeq \frac{1}{12}e^{-\frac{x^2}{2}} + \frac{1}{4}e^{-\frac{2x^2}{3}}$. Substituting (12) in (28) and integrating as in [52] the closed-form solution can be obtained as

$$P_e = \frac{\xi^2 2^{\alpha+\beta-2}}{8\pi\Gamma(\alpha)\Gamma(\beta)} \times \sum_{i=1}^{2}\left(P_i G_{6,3}^{1,6}\left(\begin{matrix}\bar{m}\\ \bar{n}\end{matrix}\middle| C_i\left(\frac{\eta A_o\sqrt{\frac{P_t T_b}{4\sigma^2}}}{\alpha\beta}\right)^2\right)\right), \tag{29}$$

where $\bar{m} = \left[\frac{1-\xi^2}{2}, \frac{2-\xi^2}{2}, \frac{1-\alpha}{2}, \frac{2-\alpha}{2}, \frac{1-\beta}{2}, \frac{2-\beta}{2}\right]$, $\bar{n} = \left[0, -\frac{\xi^2}{2}, \frac{1-\xi^2}{2}\right]$, $P_1 = \frac{1}{3}$, $P_2 = 1$, $C_1 = 8$ and $C_2 = \frac{32}{3}$. Equations (27) and (29) give BER performance of uncoded UWOC system.

B. BER CALCULATION USING KERNEL-BASED DENSITY ESTIMATION

The kernel-based density estimation is a method to estimate the PDF of the given random samples and can be used to calculate the BER. The Monte Carlo (MC) simulation method is a universal approach to estimate the BER. The drawback of this method is the large required sample size at low BER values, which results in high computational cost. In the kernel-based method [53], [54] the sample size required is smaller when compared to that of MC simulation for the same BER value. In this paper, the BER performance of SC-LDPC coded UWOC system has also been studied using the kernel-based PDF estimation [55], in addition to the MC simulation method. Let $x_i \in \{0, 1\}$ be the transmitted bits and let p_+ and p_- denote the probability that x_i is 1 and 0 respectively. The outputs available at the channel decoder are LLRs L_i, and can be written as

$$L_i = \log\left(\frac{Pr(x_i = 1|z)}{Pr(x_i = 0|z)}\right), \tag{30}$$

where z is the received signal. Let us define the soft outputs at the receiver side Y_i as

$$Y_i = Pr(x_i = 1|z) - Pr(x_i = 0|z). \tag{31}$$

Now by using (30) and (31) soft outputs can be written as

$$Y_i = \frac{1 - e^{-L_i}}{1 + e^{-L_i}}. \tag{32}$$

These are random variables with PDF as $f_Y(y)$, then the bit error probability is given by

$$p_e = p_+\int_{-\infty}^{0} f_Y^+(y)dy + p_-\int_0^\infty f_Y^-(y)dy \tag{33}$$

where f_Y^+ (respectively f_Y^-) is the conditional PDF of Y such that $x_i = 1$ (respectively $x_i = 0$). The estimation of these conditional PDFs can be obtained by [55]

$$\hat{f}_Y^+(y) = \frac{1}{N_+ h_{N_+}}\sum_{Y_i\in C_+} K\left(\frac{y - Y_i}{h_{N_+}}\right),$$
$$\hat{f}_Y^-(y) = \frac{1}{N_- h_{N_-}}\sum_{Y_i\in C_-} K\left(\frac{y - Y_i}{h_{N_-}}\right), \tag{34}$$

where C_+ and C_- are sets of received soft outputs corresponding to $x_i = 1$ and $x_i = 0$ respectively, N_+ and N_- are cardinality of C_+ and C_- respectively, h_{N_+} and h_{N_-} are smoothing parameters and $K(\cdot)$ is Kernel function. The selection of optimal smoothing parameter is important in accurately estimating the PDF. The optimal smoothing parameter based on integrated mean squared error method is given by [54]

$$h_{N_+}^* = {N_+}^{-1/5}(J(f_Y^+))^{-1/5}(M(K))^{1/5}, \tag{35}$$

where $M(K) = \int_{-\infty}^{+\infty} K^2(y)dy$, $J(f_y) = \int_{-\infty}^{+\infty}\{f_Y''(y)\}^2 dy$ and f_Y'' is second derivative of f_Y. A similar method can be used to obtain the $h_{N_-}^*$. However, smoothing parameter itself depends on unknown density function. Here we have used Gaussian

kernel $K(y) = 1/\sqrt{2\pi}\exp(-y^2/2)$, which gives the $M(K) = 1/(2\sqrt{\pi})$. By using (34), $J(\hat{f}_Y^+)$ can be obtained as

$$J(\hat{f}_Y^+) = \frac{h_{N_+}^{-5}}{N_+^2\sqrt{2}} \sum_{i=1}^{N_+}\sum_{j=1}^{N_+} K\left(\frac{Y_i - Y_j}{\sqrt{2}h_{N_+}}\right)\left[\left(\frac{Y_i - Y_j}{2h_{N_+}}\right)^4 + \frac{3}{4}\right]. \tag{36}$$

By using (35) and (36) iteratively, the optimum value of smoothing parameter $h_{N_+}^*$ can be obtained. Using a similar approach $h_{N_-}^*$ can also be obtained. Consider the first integral on the right hand side of (33). Using the first equation in (34) and applying a change of variable $\left(g = \frac{y - Y_i}{h_{N_+}}\right)$, we get

$$\begin{aligned}\int_{-\infty}^{0} \hat{f}_Y^+(y)dy &= \sum_{Y_i \in C_+} \int_{-\infty}^{\frac{-Y_i}{h_{N_+}}} \frac{1}{N_+} K(g)\, dg \\ &= \frac{1}{N_+}\sum_{Y_i \in C_+} \mathbb{Q}\left(\frac{Y_i}{h_{N_+}}\right),\end{aligned} \tag{37}$$

where $K(g)$ is Gaussian kernel and $\mathbb{Q}(\cdot)$ is Q-function. Similarly,

$$\int_{0}^{+\infty} \hat{f}_Y^-(y)dy = \frac{1}{N_-}\sum_{Y_i \in C_-} \mathbb{Q}\left(\frac{Y_i}{h_{N_-}}\right). \tag{38}$$

By substituting (37) and (38) in (33), the bit error probability can be obtained as

$$p_e = \frac{p_+}{N_+}\sum_{Y_i \in C_+} \mathbb{Q}\left(\frac{Y_i}{h_{N_+}^*}\right) + \frac{p_-}{N_-}\sum_{Y_i \in C_-} \mathbb{Q}\left(\frac{Y_i}{h_{N_-}^*}\right). \tag{39}$$

However, the accuracy of bit error probability depends on estimation of conditional PDFs in (34). These PDF estimations depend on observed soft outputs (Y_i) and smoothing parameter (h_N^*). Here we have assumed that classification of Y_i corresponding to $x_i = 1$ and $x_i = 0$ (C_+ and C_-) is known at the receiver side.

In the simulations, we have used an iterative approach to obtain $h_{N_+}^*$ using the following steps. (i) h_{N_+} is initialized with the value $(1/N_+)^{1/5}$. (ii) Using the h_{N_+} value in (36), $J(\hat{f}_Y^+)$ can be obtained. (iii) h_{N_+} is updated using (35). (iv) This iterative process continues between steps (ii) and (iii) until the difference between successive h_{N_+} values is less than 10^{-4}. After the termination of iterative process, h_{N_+} is considered as $h_{N_+}^*$. Similarly $h_{N_-}^*$ can be obtained.

The BER calculation using the kernel-based method involves the following steps. (i) Given the LLRs, the soft outputs are obtained by using (32). (ii) The soft outputs are divided into two sets C_+ and C_-. (iii) The smoothing parameters $h_{N_+}^*$ and $h_{N_-}^*$ are obtained using (35) and (36) iteratively. (iv) The bit error probability is determined using (39).

C. MULTIDIMENSIONAL P-EXIT ALGORITHM

In the literature, the decoding performance analysis of LDPC codes has been studied using the DE method [23] and the EXIT charts [24], [28]. These methods give the decoding threshold values. However, DE involves more complexity compared to the EXIT chart analysis [56], since the DE transfers the PDF information between the nodes. In [56], the traditional EXIT algorithm has been applied for the AWGN channel. In this case, the channel LLR follows the consistent Gaussian distribution (i.e. mean = variance/2), which simplifies the EXIT chart analysis. A modified multidimensional EXIT chart analysis has been studied in [57] using the Gaussian mixture model (GMM) for the power line and wireless communication hybrid fading channel. In our study, we have used this GMM approach along with modifications to the P-EXIT chart analysis carried out in [28]. Our approach is applicable to the memoryless binary-input symmetric-output channels and is described below.

The LLR values received from the GG-PE channel follow a distribution which is complex to analyze. Therefore, we have used the GMM model with the Expectation-Maximization algorithm [58] to fit the LLR distribution with a mixture of Gaussian components. The PDF of Gaussian mixture (GM) can be written as

$$f_L(l) = \sum_{g=1}^{G} \frac{w_g}{\sqrt{2\pi\sigma_g^2}} exp\left(-\frac{(l-\mu_g)^2}{2\sigma_g^2}\right) \tag{40}$$

where G is the number of Gaussian components in the mixture, and w_g, μ_g and σ_g^2 are the weight, mean and variance of the g^{th} Gaussian component respectively. The obtained Gaussian components do not follow the consistent Gaussian distribution. However, the P-EXIT chart analysis study in [28] is for the consistent Gaussian distributions. Therefore, we have modified the P-EXIT algorithm, for the case where the Gaussian distribution does not follow the relation of variance being twice the mean value.

The EXIT algorithm calculates the mutual information (MI) between the message variable X and the channel LLR. If the LLR distribution is the sum of Gaussian components, then the MI can be obtained as

$$I(X;L) = \sum_{g=1}^{G} w_g I(X;L_g), \tag{41}$$

where

$$\begin{aligned} I(X;L_g) &= 1 - \int_{-\infty}^{+\infty} \left(\frac{exp\left(-\frac{(l-\mu_g)^2}{2\sigma_g^2}\right)}{\sqrt{2\pi\sigma_g^2}}\right) \\ &\quad \times \log_2\left(1 + exp\left(-\frac{2\mu_g l}{\sigma_g^2}\right)\right) dl \\ &= J'(\mu_g, \sigma_g). \end{aligned} \tag{42}$$

The $J'(\mu_g, \sigma_g)$ will become $J(\sigma_g)$ for the case of $2\mu_g = \sigma_g^2$, which is a case with consistent Gaussian distribution in the traditional EXIT approach. The numerical solution of $J'(\mu_g, \sigma_g)$ can be obtained by using the Gauss-Hermite

quadrature method [59], and is given below

$$J'(\mu_g, \sigma_g) = 1 - \frac{1}{\sqrt{\pi}} \times \sum_{u=1}^{U} \left(c_u \times \log_2 \left[1 + exp\left(\frac{-2\mu_g}{\sigma_g^2} \times \left(\sqrt{2} a_u \sigma_g + \mu_g \right) \right) \right] \right) \tag{43}$$

where c_u is weight, a_u is abscissa zero and U is the Hermite integral order.

The multidimensional modified P-EXIT analysis involves the following steps for the protograph based LDPC code with base matrix B. It is assumed that the dimension of B is $M \times N$ and the elements in B are $[b_{ij}]$.

1) INITIALIZATION

The LLR information passed from a variable node j to a check node i can be calculated using (24). It is assumed that the output from the check node satisfies the approximate Gaussian distribution. In this case, the output LLR from a variable node is a mixture of Gaussian distributions. Therefore, the mean and variance of this distribution at each iteration satisfy the following relations

$$\mu_{vc,g}^{j\to i}(l) = \sum_{k=1}^{M} (b_{kj} - \delta_{ki}) \mu_{cv,g}^{k\to j}(l-1) + \mu_{ch,g}^{j} \tag{44}$$

$$\sigma_{vc,g}^{2\ \ j\to i}(l) = \sum_{k=1}^{M} (b_{kj} - \delta_{ki}) \sigma_{cv,g}^{2\ \ k\to j}(l-1) + \sigma_{ch,g}^{2\ \ j} \tag{45}$$

where g represents the g^{th} Gaussian component, l is the iteration number, b_{kj} is the element in B (i.e. number of edges connected between variable node j and check node k) and δ_{ki} is 1 for $i = k$ and 0 for $i \neq k$. The subscripts vc, cv and ch represent the variable node to check node, check node to variable node and channel information respectively. In the first iteration $\mu_{cv,g} = 0$ and $\sigma_{cv,g}^2 = 0$. If the variable node of type j is punctured, then $\mu_{ch,g}^{j}$ and $\sigma_{ch,g}^{2\ \ j}$ are considered as zero.

2) VARIABLE NODE TO CHECK NODE UPDATE

In the protograph, each variable node of type j sends extrinsic MI to check node of type i which can be written as

$$I_{EV,g}^{j\to i} = J'(\mu_{vc,g}^{j\to i}, \sigma_{vc,g}^{j\to i}) \tag{46}$$

where $\mu_{vc,g}^{j\to i}$ and $\sigma_{vc,g}^{j\to i}$ can be obtained by using (44) and (45) respectively. The overall MI can be written as

$$I_{EV}^{j\to i} = \sum_{g=1}^{G} w_g I_{EV,g}^{j\to i} \tag{47}$$

3) CHECK NODE TO VARIABLE NODE UPDATE

If the LLRs received from the variable nodes at the input to a check node are assumed to have the Gaussian distribution, then MI from the check node of type i to a variable node of type j can be written as

$$I_{EC,g}^{i\to j} = 1 - J\left(\sqrt{\sum_{k=1}^{N} (b_{ik} - \delta_{kj}) \left(J^{-1}(1 - I_{EV,g}^{j\to i}) \right)^2} \right) \tag{48}$$

where $J(\cdot)$ and $J^{-1}(\cdot)$ can be obtained numerically as given in [24]. The mean and variance of the output information from each check node can be obtained as

$$\mu_{cv,g}^{i\to j} = \frac{\left(J^{-1}\left(I_{EC,g}^{i\to j} \right) \right)^2}{2}, \tag{49}$$

$$\sigma_{cv,g}^{2\ \ i\to j} = \left(J^{-1}\left(I_{EC,g}^{i\to j} \right) \right)^2. \tag{50}$$

These values for the mean and variance will be used in (44) and (45) to update the mean and variance of LLR information at the output of a variable node of type j. The overall MI from a check node of type i to a variable node of type j can be written as

$$I_{EC}^{i\to j} = \sum_{g=1}^{G} w_g I_{EC,g}^{i\to j}. \tag{51}$$

4) OVERALL MUTUAL INFORMATION

The complete MI at a variable node of type j corresponding to the g^{th} Gaussian component can be written as

$$I_{CMI,g}^{j} = J'\left(\sum_{k=1}^{M} \mu_{cv,g}^{k\to j} + \mu_{ch,g}^{j}, \sqrt{\sum_{k=1}^{M} b_{kj} \sigma_{cv,g}^{2\ \ k\to j} + \sigma_{ch,g}^{2\ \ j}} \right) \tag{52}$$

Now the overall MI at a variable node of type j is

$$I_{CMI}^{j} = \sum_{g=1}^{G} w_g I_{CMI,g}^{j} \tag{53}$$

At each iteration, I_{CMI}^{j} is calculated for each variable node of type j. If $I_{CMI}^{j} = 1$ for every j with set precision, then the algorithm stops; otherwise it goes to step-2.

The divide and conquer method has been used to find the threshold value of transmitted power $p_t^* = \min\{p_t : I_{CMI}^{j} = 1, \forall j\}$. In this method, the observation interval of p_t is selected such that p_t^* lies within this interval. Let $[p_i, p_f]$ be the observation interval. The algorithm starts with initial power of $\frac{p_i+p_f}{2}$. If the condition $I_{CMI}^{j} = 1, \forall j$ is satisfied, then it selects the interval as $[p_i, \frac{p_i+p_f}{2}]$, else it selects the interval as $[\frac{p_i+p_f}{2}, p_f]$. This process continues until a specified precision for p_t^* is obtained. In our analysis, this precision has been set to two digits after the decimal point.

The decoding thresholds obtained by using the multidimensional modified P-EXIT analysis are given in Table 1 for different channel parameters and code rates. It is observed that the decoding threshold decreases as turbulence strength

TABLE 1. Optimum values of threshold in dB for different channel conditions and code rates.

Channel parameters		Rate=1/2	Rate=3/4	Rate=4/5
SI=1.145	$\xi = 2.3$	0.13	5.07	6.62
	$\xi = 1.25$	3.47	9.24	11.29
	$\xi = 1$	6.12	13.12	15.87
SI=0.6946	$\xi = 2.3$	-0.97	2.13	3.21
	$\xi = 1.25$	2.57	6.48	8.53
	$\xi = 1$	5.08	10.41	13.28
SI=0.2094	$\xi = 2.3$	-2.08	-1.37	-0.89
	$\xi = 1.25$	1.02	3.06	4.23
	$\xi = 1$	3.14	6.91	8.34

decreases for a given pointing error parameter (ξ) value. Similarly for a given σ_I^2, the decoding threshold increases as ξ value decreases.

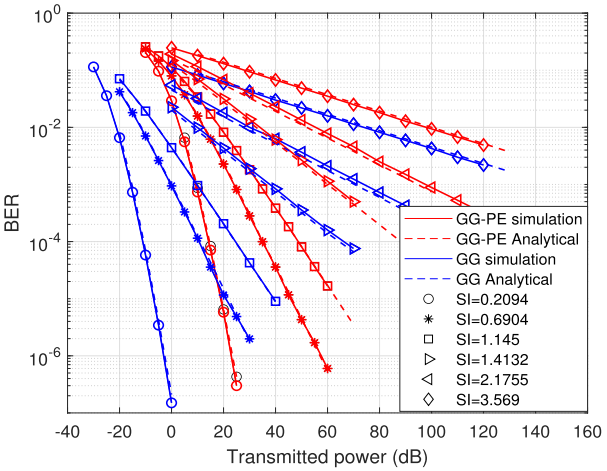

FIGURE 11. Performance of an uncoded UWOC system over the Gamma-Gamma channel with and without pointing errors using the analytical method and the simulation approach.

V. RESULTS AND DISCUSSION

The UWOC channel model that we have considered is strong turbulence with pointing errors. The parameter values that we have considered in calculating the channel effects are from [35], and a link length of 30 m has been considered to account for strong turbulence with the following parameters, wavelength $\lambda = 530\ nm$, $\epsilon = 2 \times 10^{-8}\ m^2/s^3$, $\omega = -0.03$, $\chi_T = 10^{-4}\ K^2/s$ and $\sigma_I^2 = 1.145$. The corresponding α, β values are 4.2257, 1.3622 respectively. The pointing error effects are included by considering $A_0 = 0.0764$ and ${\sigma_s}^2 = 0.2075 \times 10^{-3}\ m^2$, $\Omega_{z_{eq}} = 66.5 \times 10^{-3}\ m$, which results in $\xi = 2.3$. We have also considered the $\sigma_I^2 = 0.6946,\ 0.2094$ to observe the performance in moderate, weak turbulence cases [8], [9] along with other pointing error values $\xi = 1.5,\ 1.25,\ 1$.

All the simulations have been performed using the MATLAB. First, the parity-check matrix of the SC-LDPC code is obtained through the PEG algorithm. Then, the data is encoded using the partial syndrome former method, which utilizes the parity check matrix. Once the data is encoded, it is transmitted through the channel. Finally, the received data is decoded using the sliding window decoding method. In the simulations, the Acceptance-Rejection (A-R) method [60] has been used to obtain the random samples from the PDF of I_p. The PDF of I_t is represented by the GG distribution. Samples from the GG distribution can be generated by multiplying the samples from two independent Gamma distributions (one with parameter α and another with parameter β). The *gamrnd* MATLAB function has been used to generate the samples from the Gamma distribution. To model the channel fading, samples obtained from the PDFs of I_p and I_t are used in (2).

The implementation of A-R method to generate a sample X from the PDF $f(x)$ uses the following steps. (i) Generate a sample Y from the known PDF $g(y)$ for which there is a well known procedure to generate samples. (ii) Generate a sample U from the uniform distribution ([0,1]). (iii) If $U \leq \frac{f(Y)}{cg(Y)}$ then set $X = Y$, otherwise go to step (i), where c is a constant greater than 1 such that $\sup_x \left\{\frac{f(x)}{g(x)}\right\} \leq c$. The selected samples X follow the PDF $f(x)$. In our simulations $c = 5.21$ is used to generate samples from the PDF of I_t, where $g(x)$ considered as a uniform distribution.

In [18] and [19], the performance of a strong turbulent UWOC system has been studied using ϵ, ω and the SNR values. In [17], the nephelometric turbidity unit has been used as the turbulence strength and the BER performance is studied at different transmitted power values. In [8] and [9], different σ_I^2 values have been used to indicate the different turbulence strengths. In our analysis, σ_I^2 is used to indicate the turbulence strength and the performance of system is studied for different transmitted power values. The performance of the uncoded OOK modulated UWOC system over the GG channel and that over the GG channel with pointing errors (GG-PE) has been obtained by using the analytical methods ((27), (29)), as well as the simulation approach for different σ_I^2 values and is shown in Fig. 11. It is observed that the performance of the analytical methods is consistent with the simulation approach over both the channel models (GG and GG-PE). Furthermore, it is observed that as the σ_I^2 value increases the performance of the link deteriorates. Thus, increased turbulence results in degraded performance. Also, it is observed from the results that to achieve a BER of 10^{-4}, the transmitted power required over the GG channel is 24.5 dB and that over the GG-PE channel is 48.7 dB (i.e. the performance gap is 24.2 dB) for the given $\sigma_I^2 = 1.145$ and $\xi = 2.3$. The required transmitted power increases as the turbulence strength increases. It is observed that the required power to achieve a BER of 10^{-4}, for low turbulence (SI = 0.2094), moderate turbulence (SI = 0.6946) and high turbulence (SI = 1.145) is 14.23 dB, 35 dB, 48.7 dB respectively for a given $\xi = 2.3$.

The BER performance of rate 1/2 SC-LDPC coded system for different channel parameters (σ_I^2 and ξ) and channel models has been studied using kernel-based PDF estimation

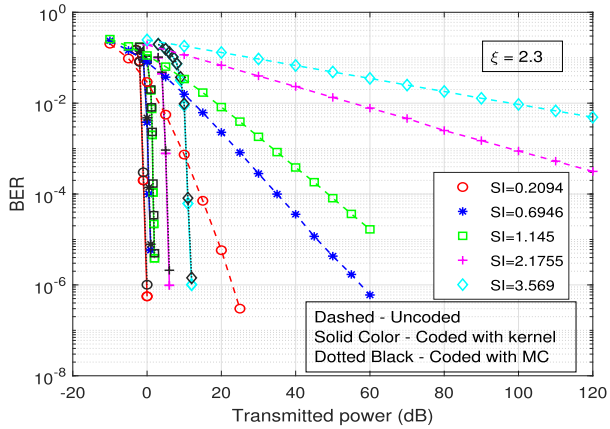

FIGURE 12. Performance comparison of rate 1/2 SC-LDPC coded and uncoded GG-PE links ($\xi = 2.3$) for different SI values.

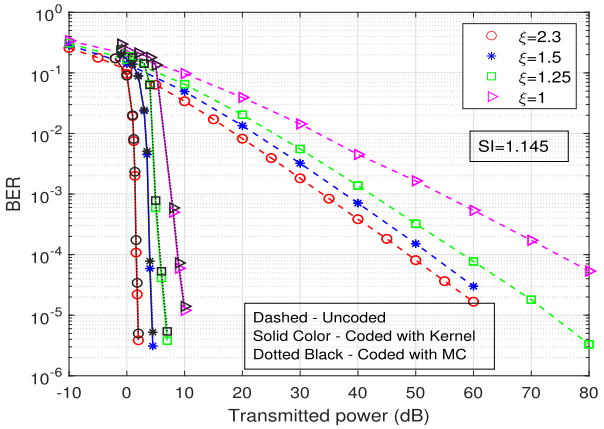

FIGURE 14. Performance comparison of rate 1/2 SC-LDPC coded and uncoded GG-PE links ($\sigma_I{}^2 = 1.145$) for different pointing error values.

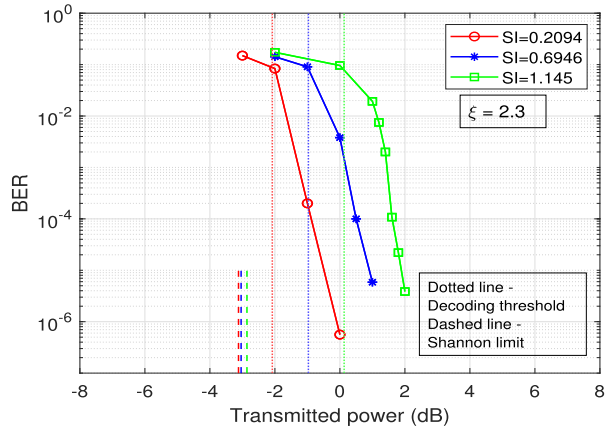

FIGURE 13. Decoding threshold (indicated by dotted vertical line) and BER performance of rate 1/2 SC-LDPC coded GG-PE links ($\xi = 2.3$) for different SI values.

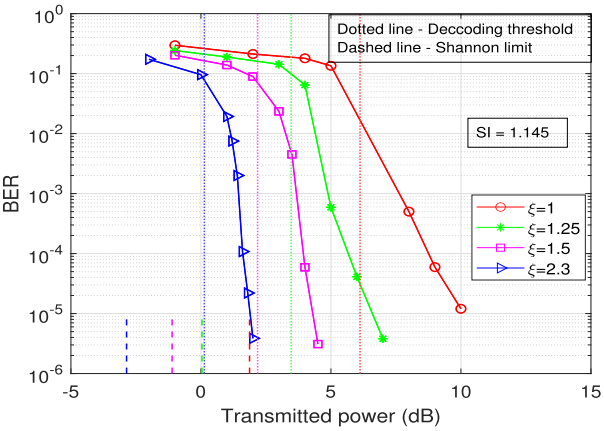

FIGURE 15. Decoding threshold (indicated by dotted vertical line) and BER performance of rate 1/2 SC-LDPC coded GG-PE links ($\sigma_I{}^2 = 1.145$) for different pointing error values.

method and MC simulations. Furthermore, for a given turbulence strength $\sigma_I^2 = 1.145$ and pointing error $\xi = 2.3$, performance of SC-LDPC codes for different code rates has been studied using the kernel-based method and MC simulations. From the results, it is observed that these two methods are consistent with each other.

The performance of the rate 1/2 SC-LDPC code has been studied for different σ_I^2 values over the GG-PE channel for a given $\xi = 2.3$ using MC simulations and kernel-based method and is shown in Fig. 12. Here $M = 256$ and $w = 1$ have been used. It is observed that the SC-LDPC code gives a coding gain of 47 dB, 34.5 dB and 15.1 dB for σ_I^2 values of 1.145, 0.6946 and 0.2094 respectively at a BER of 10^{-4}. The observed coding gain is significant in the presence of moderate and strong turbulence conditions.

The decoding threshold of ARJA protograph based SC-LDPC code obtained over GG-PE link with SI values of $\sigma_I^2 = 1.145, 0.6946, 0.2094$ for a given $\xi = 2.3$ is shown in Fig.13. These decoding threshold values are indicated by vertical dotted lines in the plot. The gap between the threshold and waterfall curve is because of the SC-LDPC code selected from the code ensemble and the finite length codeword considered in the simulation in contrast to asymptotic analysis of EXIT chart. It is observed that at a BER of 10^{-5}, there is a gap of 1.76 dB between the BER curve and decoding threshold for the GG-PE link with $\sigma_I^2 = 1.145$ and $\xi = 2.3$. Also, the Shannon limit for different turbulence strengths are shown in Fig. 13 using a short dashed vertical line. It is observed that the variation in the Shannon limit for different turbulence strengths is very small compared to the variation in the decoding threshold obtained by the EXIT chart.

The performance of rate 1/2 SC-LDPC code has also been studied for different values of ξ for $\sigma_I^2 = 1.145$ and is shown in Fig. 14. Here $C_A(0)$ ensemble with $M = 256$ and $w = 1$ has been used. It is observed that the performance of the system degrades as ξ value decreases. This is because, for a given value of equivalent beam width, the decrease in the value of ξ results in increased displacement standard deviation. The SC-LDPC code gives a coding gain of 65.84 dB, 52.54 dB, 48.65 dB, 47 dB for ξ values of 1, 1.25, 1.5, 2.3 respectively at a BER of 10^{-4}. In uncoded system, a lower value of ξ corresponds to increased pointing errors. It is observed that

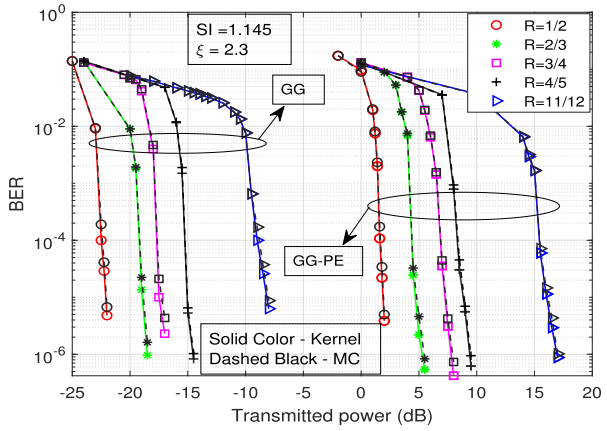

FIGURE 16. Performance comparison of SC-LDPC codes for different code rates over the Gamma-Gamma channel with and without pointing errors ($\sigma_I^2 = 1.145$, $\xi = 2.3$).

the additional power requirement is 3.87 dB, 5.63 dB and 16.42 dB when ξ changes from 2.3 to 1.5, 1.5 to 1.25 and 1.25 to 1 respectively. Thus, the additional power requirement to achieve a required BER value increases rapidly as ξ value decreases.

The decoding thresholds obtained for different ξ values for a given turbulence strength of $\sigma_I^2 = 1.145$ are shown in Fig. 15. It is observed that the gap between the BER curve and threshold is 1.76 dB and 3.33 dB at a BER of 10^{-5} for $\xi = 2.3$ and $\xi = 1.25$ respectively. Also, it is observed that the gap between the threshold and Shannon limit is 2.99 dB, 3.29 dB, 3.43 dB and 4.25 dB for ξ values of 2.3, 1.5, 1.25 and 1 respectively. The decoding threshold value increases as the pointing error parameter ξ value decreases for a given SI value. When ξ changes from 2.3 to 1.5, 1.5 to 1.25 and 1.25 to 1, the increment in the decoding threshold is 2.05 dB, 1.29 dB and 2.65 dB respectively for a given $\sigma_I^2 = 1.145$.

The different code rate ensembles $C_A(n)$ with $M = 256$, $w = 1$, $L = 10$ have been obtained by using AR4JA protographs with $n = 0$, 1, 2, 3 and 10. The performance of different code rate ensembles is compared over the both channel models and is shown in Fig. 16. It is observed that the performance gap between GG and GG-PE channels with a rate 1/2 SC-LDPC code is 24 *dB* at BER of 10^{-4}. This performance gap shows the significance of considering pointing errors in the performance evaluation of UWOC system.

The performance of these $C_A(n)$ ensembles has also been observed for the code rates of 1/2, 3/4 and 4/5 with different combinations of ${\sigma_I}^2$ and ξ values and is shown in Fig. 17. From Fig. 17a, it is observed that for a given ${\sigma_I}^2 = 1.145$, a change in ξ value from 2.3 to 1 shows the performance deviation of 7.1 *dB*, 8.6 *dB* and 9.4 *dB* for SC-LDPC codes with rate 1/2, 3/4 and 4/5 respectively. Similar types of observations can be drawn from Fig. 17b and Fig. 17c for the ${\sigma_I}^2$ values of 0.6946 and 0.2094 respectively. The rate 1/2 SC-LDPC code performance for different combinations

TABLE 2. Required transmitted power in dB to achieve a BER of 10^{-4} for different channel conditions and code rates.

Channel parameters		Rate=1/2	Rate=3/4	Rate=4/5
SI=1.145	$\xi = 2.3$	1.65	6.89	8.34
	$\xi = 1.25$	5.67	11.24	13.62
	$\xi = 1$	8.75	15.49	17.74
SI=0.6946	$\xi = 2.3$	0.51	3.72	4.62
	$\xi = 1.25$	4.42	8.43	10.61
	$\xi = 1$	7.11	12.31	15.33
SI=0.2094	$\xi = 2.3$	-0.85	0.21	0.72
	$\xi = 1.25$	2.67	4.62	5.61
	$\xi = 1$	5.15	8.61	10.32

of ${\sigma_I}^2$ and ξ values is shown in Fig. 17d. It is observed that a change in ${\sigma_I}^2$ value from 1.145 to 0.2094 shows a performance deviation of 2.5 *dB*, 3 *dB* and 3.6 *dB* for ξ values of 2.3, 1.25 and 1 respectively.

The decoding thresholds for different code rates over the GG-PE link with $\sigma_I^2 = 1.145$ and $\xi = 2.3$ are shown in Fig. 18. It is observed that as the code rate increases, the threshold value and Shannon limit also increase. The decoding threshold obtained for rate 1/2, 2/3, 3/4 and 4/5 code is 0.13 dB, 2.86 dB, 5.07 dB and 6.62 dB respectively.

The performance of the SC-LDPC coded UWOC system for different channel parameters and code rates is summarized in Table 2. This table gives the required transmitted power in dB to achieve a BER of 10^{-4} for different channel parameters and code rates.

The different statistical distributions for fading in an UWOC turbulent channel studied in [9] through experimental results are log-normal (LN), exponential log-normal (ELN), weibull (WBL), exponential weibull (EWBL), GG and generalized Gamma (Gen-G). We have used the A-R method to generate the samples from these distributions using the corresponding PDFs. In [8] and [9], it is noted that for $\sigma_I^2 > 1$, the GG channel model has a better fit with the measured data. The performance of rate 1/2 SC-LDPC code ($C_A(0)$ with $M = 256$ and $W = 4$) over these channel models with and without pointing errors for $\sigma_I^2 = 1.145$ and $\xi = 2.3$, is shown in Fig. 19. It is observed that the performance over GG channel is close to the performance over WBL channel and the remaining channel models show deviation from these two channel models for both the cases.

The performance of rate 1/2 SC-LDPC code over the GG-PE channel with $\xi = 2.3$ has been studied for different values of W and M. Fig. 20 shows the BER curves for different values of W over the GG-PE channel with different σ_I^2 values. The value of $M = 256$ is fixed and $W = 3$, 4, 5 and 6 have been used. From Fig. 20, it is observed that the performance of SC-LDPC code is improved by 1.7 *dB* by increasing the W value from 3 to 6 for the case of $\sigma_I^2 = 1.145$ at a BER of 10^{-4}. However, the increase in W results in increased decoding latency.

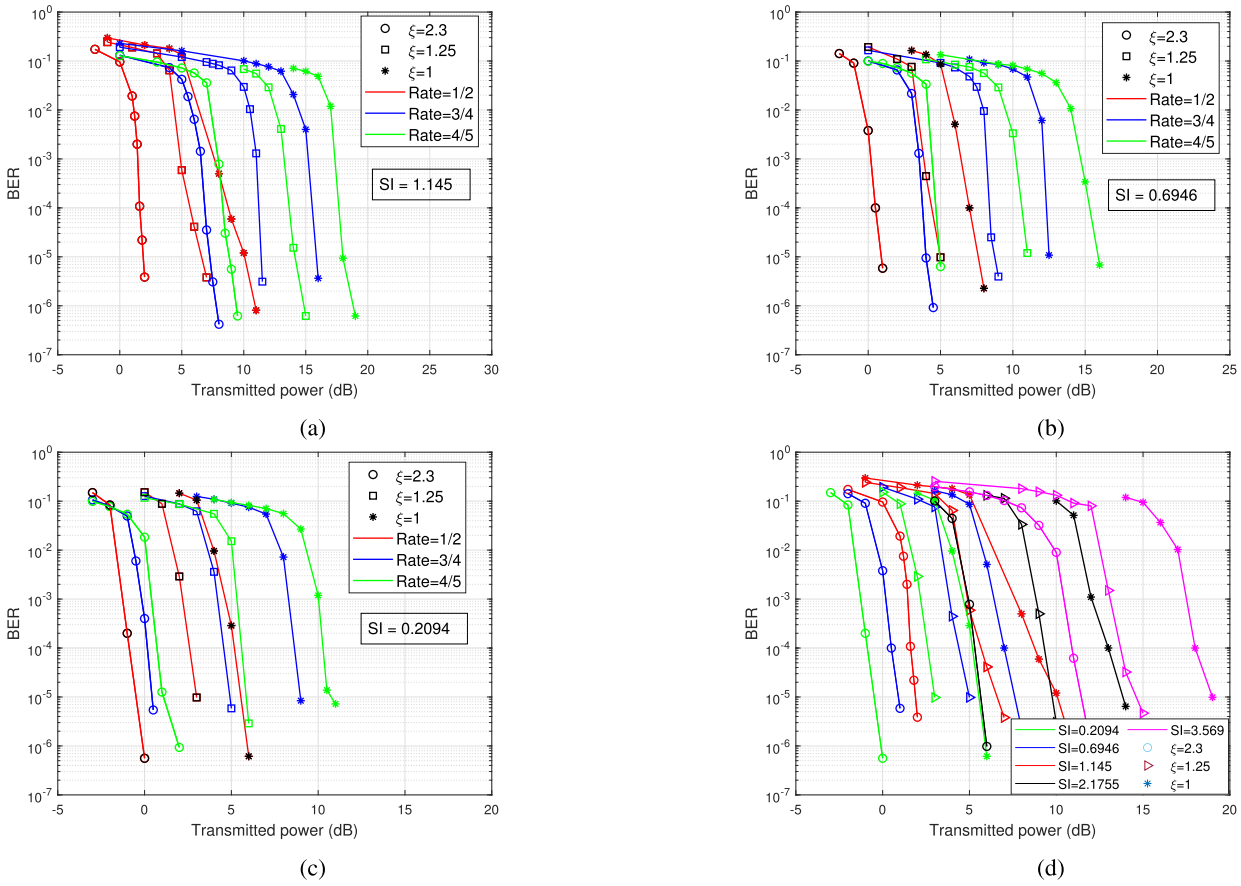

FIGURE 17. Performance comparison of SC-LDPC codes over the Gamma-Gamma channel with pointing errors. (a) $\sigma_I^2 = 1.145$, (b) $\sigma_I^2 = 0.6946$, (c) $\sigma_I^2 = 0.2094$ for different code rates and (d) for rate 1/2 code with different σ_I^2, ξ values.

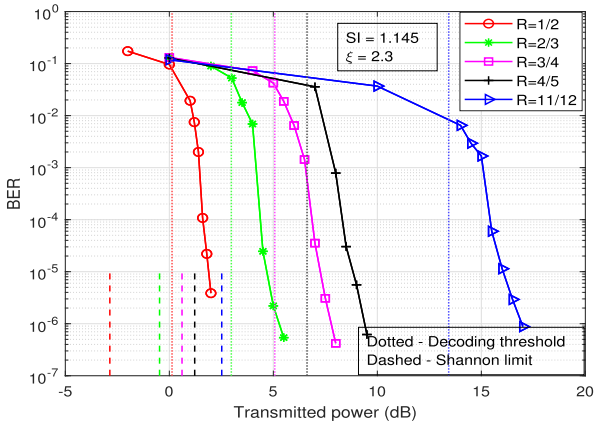

FIGURE 18. BER performance of SC-LDPC codes for different code rates over the Gamma-Gamma channel with pointing errors ($\sigma_I^2 = 1.145$, $\xi = 2.3$) with decoding thresholds indicated by dotted vertical lines.

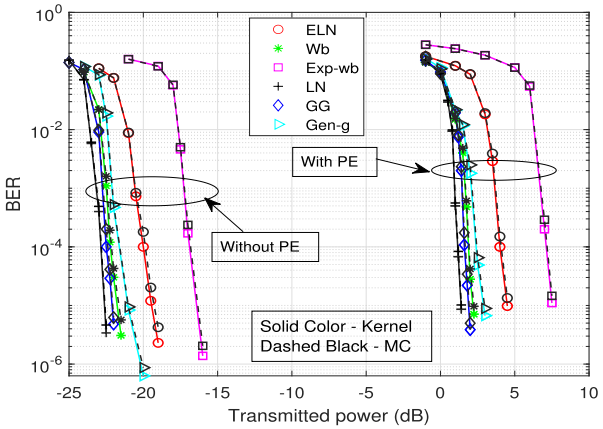

FIGURE 19. Performance comparison of rate 1/2 SC-LDPC code over different channel models with and without pointing errors ($\sigma_I^2 = 1.145$, $\xi = 2.3$).

The plot in Fig. 21 shows the required transmitted power to achieve a BER of 10^{-4} under different decoding latency values. It is observed that the required power decreases with an increase in W (latency). However, the quantum of reduction also decreases with an increase in W. That is for large values of window length there is only negligible performance improvement. However, the complexity increases with the window length.

The BER curves for different M values of rate 1/2 SC-LDPC code over the GG-PE channel model are shown in Fig. 22. It is observed that the performance of the system improves with the increase in the value of M.

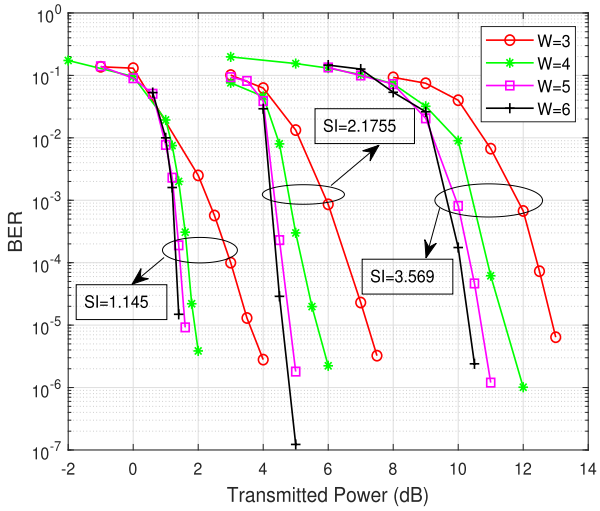

FIGURE 20. Performance comparison of rate 1/2 SC-LDPC codes over the Gamma-Gamma channel with pointing errors under different window lengths and σ_I^2 values.

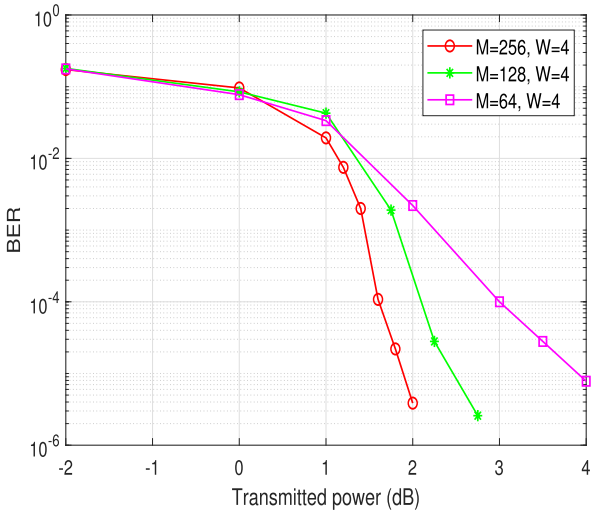

FIGURE 22. Performance comparison of ARJA protograph based rate 1/2 SC-LDPC codes over Gamma-Gamma channel with pointing errors ($\sigma_I^2 = 1.145$, $\xi = 2.3$) for different graph lifting factors.

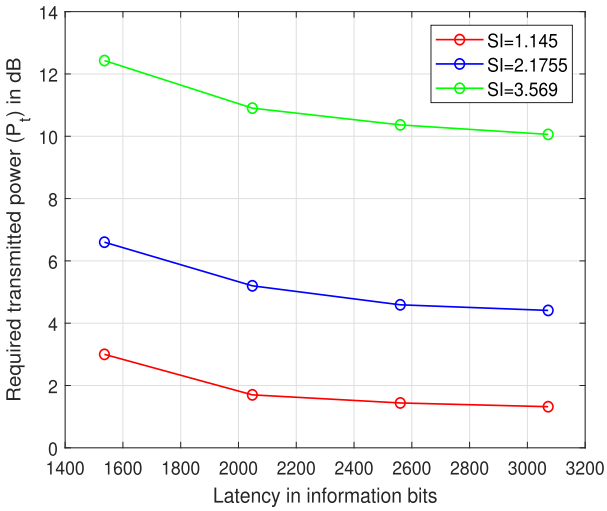

FIGURE 21. The required transmitted power to achieve a BER of 10^{-4} for different values of decoding latency for different σ_I^2 values.

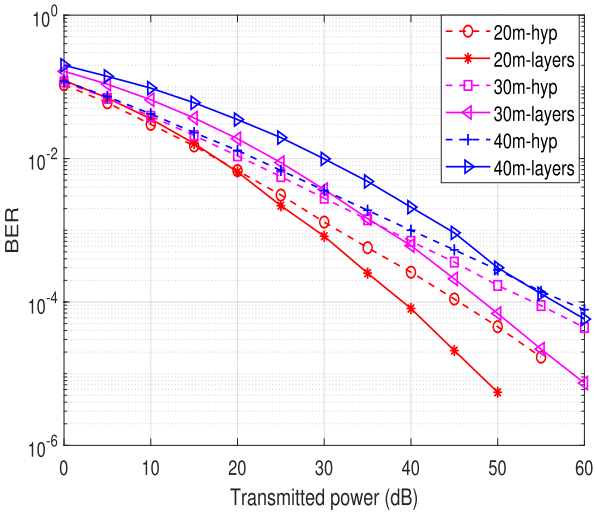

FIGURE 23. Performance comparison of hypothetical and cascaded channel models for uncoded vertical links with different depths and layers.

The performance of SC-LDPC coded UWOC system over a vertical link has also been studied by using the parameters of the channel in [61]. We have used ARJA based SC-LDPC code with $M = 256$, $L = 10$, $w = 1$ and $W = 4$. A hypothetical channel model with a single layer and a cascaded channel model with multiple (k) layers have been considered. Here thickness of each layer in the cascaded channel model has been considered to be 10 m. The link lengths considered are 20 m, 30 m and 40 m. The corresponding (α,β) parameter values for the hypothetical channel model are (4.08,1.47), (4.70,1.21) and (5.45,1.12). In the case of the cascaded channel model, the three link lengths have been modeled using 2, 3 and 4 layers respectively. The corresponding channel parameter values (α_j,β_j) are (4.59,2.82), (4.64,2.88), (4.70,2.96) and (4.77,3.05), where $j = 1, 2, ..k$ for the channel with k layers. The performance of uncoded hypothetical and cascaded channel models is shown in Fig. 23. It is observed that when compared with the cascaded channel model, the hypothetical channel model underestimates the BER values in the low SNR region and overestimates them in the high SNR region.

The performance of SC-LDPC code over these two channel models is shown in Fig. 24. It is observed that the hypothetical channel model always underestimates the BER values when compared to the cascaded model. Furthermore, it is observed that at a BER of 10^{-4} the performance gap is 1.1 dB for a link length of 20 m, whereas it increases to 5.5 dB when the link length is increased to 40 m. This increase in performance gap shows the importance of cascaded channel model for long link lengths of coded UWOC vertical link. The decoding

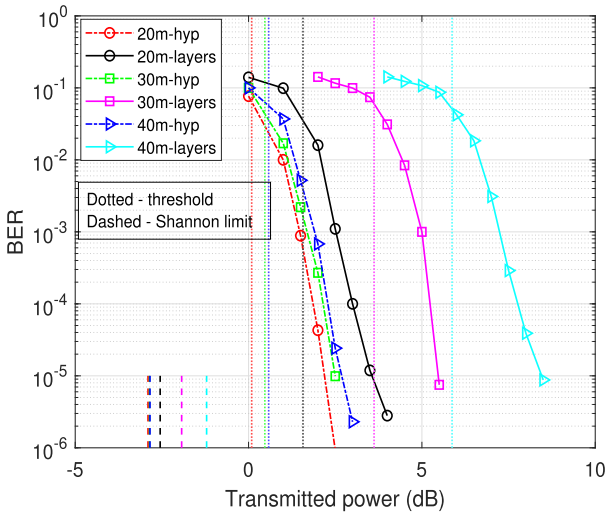

FIGURE 24. Performance comparison of hypothetical and cascaded channel models for rate 1/2 SC-LDPC coded vertical links with different depths and layers.

threshold and Shannon limit are shown in Fig. 24 using a dotted vertical line and a dashed vertical line respectively. It is observed that as the number of layers increase the decoding threshold increases.

The observations from our investigation study can be summarized as follows. (i) The BER performance of the SC-LDPC coded system obtained by using the MC simulations is consistent with the kernel-based density estimation approach. (ii) The kernel-based density estimation approach has the advantage of lower complexity since the sample size required is smaller than that of the MC simulations. (iii) From the results of SC-LDPC coded UWOC system, it is observed that the coding gain is significant in the case of strong and moderate turbulence compared to the case of low turbulence, for a given pointing error parameter ξ. (iv) Corresponding to different turbulent strengths, the variation in the Shannon limit is very small compared to the variation in the decoding thresholds. The gap between the decoding threshold and the Shannon limit increases with the turbulence strength. (v) The BER performance over the GG channel is close to that over the WBL channel under strong turbulence. (vi) The performance gap between the GG channel and GG-PE channel is significant. This gap shows the importance of considering pointing errors in the analysis of system performance. (vii) In the uncoded system, the required transmitted power to achieve a given BER increases rapidly as the pointing error parameter ξ decreases. In the coded system the coding gain is higher when ξ is smaller. (viii) The performance of SC-LDPC code improves with the decoding window length. However, the quantum of improvement decreases as the window length increases. On the other hand, the complexity increases with the window length. (ix) The performance of the SC-LDPC coded UWOC system increases with the graph lifting factor, since it increases the codeword length. (x) From the performance of the vertical link, it is observed that the gap between the performance of the cascaded channel model and the hypothetical channel model increases as the link length increases. This increase in performance gap suggests the importance of a cascaded channel model for long link length in a coded UWOC vertical link.

The following assumptions have been made in our investigation, and have to be checked for the application of the results. (i) The strong turbulence channel has been modeled as having GG distribution. (ii) In obtaining the channel fading coefficients due to pointing errors, the PDF of the displacement of the beam at the detector has been considered as Rayleigh distribution. (iii) A sample code has been considered from the ensemble of SC-LDPC codes, which may result in a small variation from the performance of other codes in the ensemble. (iv) The analytical BER closed form expression is derived over the uncoded UWOC channel for the case of strong turbulence with GG distribution and pointing errors. Furthermore, it is to be noted that the multi dimensional modified P-EXIT algorithm is applicable to memoryless binary-input symmetric-output channels.

VI. CONCLUSION

The UWOC system with strong turbulence and pointing errors has been studied in this paper. The performance of SC-LDPC codes has been investigated over the GG-PE channel for different turbulence strengths, pointing error values and for various code rates and encoder and decoder parameters. Different channel models have also been considered. It is observed that, the rate 1/2 ARJA protograph based SC-LDPC code with $M = 256$, $L = 10$, $w = 1$ achieves a coding gain of 47 dB at a BER of 10^{-4} for strong turbulence ($\sigma_I^2 = 1.145$) channel model with pointing errors ($\xi = 2.3$). From the performance of vertical link, it is observed that as the link length increases from 20 m to 40 m the performance gap between hypothetical and cascaded channel models increases from 1.1 dB to 5.5 dB. The different code rate ensembles have been obtained using AR4JA protographs. The results also show that the performance of the SC-LDPC code is improved by 1.7 dB by increasing the window length from 3 to 6 keeping the graph lifting factor constant. However, the quantum of improvement in performance decreases with the increase in the window length. A performance improvement of 1.4 dB is observed by increasing the value of the graph lifting factor from 64 to 256 keeping the window length constant. As for future work, the following may be considered. (i) Protographs may be constructed to reduce the gap between the threshold value and the Shannon limit. (ii) Since pointing errors cause significant degradation in performance over the strong turbulent channel, schemes that reduce the pointing errors may be studied. (iii) Performance of the UWOC vertical link may be investigated in detail.

REFERENCES

[1] G. Schirripa Spagnolo, L. Cozzella, and F. Leccese, "Underwater optical wireless communications: Overview," *Sensors*, vol. 20, no. 8, p. 2261, Apr. 2020.

[2] X. Sun, C. H. Kang, M. Kong, O. Alkhazragi, Y. Guo, M. Ouhssain, Y. Weng, B. H. Jones, T. K. Ng, and B. S. Ooi, "A review on practical considerations and solutions in underwater wireless optical communication," *J. Lightw. Technol.*, vol. 38, no. 2, pp. 421–431, Jan. 15, 2020.

[3] C.-C. Kao, Y.-S. Lin, G.-D. Wu, and C.-J. Huang, "A comprehensive study on the Internet of Underwater Things: Applications, challenges, and channel models," *Sensors*, vol. 17, no. 7, p. 1477, Jun. 2017.

[4] Y. Alharbi and A. Ahmad, "Underwater Internet of Things to analyse oceanic data," *IETE J. Res.*, vol. 69, pp. 1–14, Mar. 2022.

[5] N. Saeed, A. Celik, T. Y. Al-Naffouri, and M.-S. Alouini, "Underwater optical wireless communications, networking, and localization: A survey," *Ad Hoc Netw.*, vol. 94, Nov. 2019, Art. no. 101935.

[6] M. A. Al-Habash, "Mathematical model for the irradiance probability density function of a laser beam propagating through turbulent media," *Opt. Eng.*, vol. 40, no. 8, p. 1554, Aug. 2001.

[7] R. A. Leathers, T. V. Downes, C. O. Davis, and C. D. Mobley, "Monte Carlo radiative transfer simulations for ocean optics: A practical guide," Nav. Res. Lab Washington DC Appl. Opt. Branch, Washington, DC, USA, Tech. Rep. 426624, 2004.

[8] M. V. Jamali, P. Khorramshahi, A. Tashakori, A. Chizari, S. Shahsavari, S. AbdollahRamezani, M. Fazelian, S. Bahrani, and J. A. Salehi, "Statistical distribution of intensity fluctuations for underwater wireless optical channels in the presence of air bubbles," in *Proc. Iran Workshop Commun. Inf. Theory (IWCIT)*, May 2016, pp. 1–6.

[9] M. V. Jamali, A. Mirani, A. Parsay, B. Abolhassani, P. Nabavi, A. Chizari, P. Khorramshahi, S. Abdollahramezani, and J. A. Salehi, "Statistical studies of fading in underwater wireless optical channels in the presence of air bubble, temperature, and salinity random variations," *IEEE Trans. Commun.*, vol. 66, no. 10, pp. 4706–4723, Oct. 2018.

[10] H. G. Sandalidis, T. A. Tsiftsis, and G. K. Karagiannidis, "Optical wireless communications with heterodyne detection over turbulence channels with pointing errors," *J. Lightw. Technol.*, vol. 27, no. 20, pp. 4440–4445, Oct. 15, 2009.

[11] P. Saxena and M. R. Bhatnagar, "A simplified form of beam spread function in underwater wireless optical communication and its applications," *IEEE Access*, vol. 7, pp. 105298–105313, 2019.

[12] Z. Lin, G. Xu, Q. Zhang, and Z. Song, "Average symbol error probability and channel capacity of the underwater wireless optical communication systems over oceanic turbulence with pointing error impairments," *Opt. Exp.*, vol. 30, no. 9, p. 15327, 2022.

[13] R. Boluda-Ruiz, A. García-Zambrana, B. Castillo-Vázquez, and S. Hranilovic, "Impact of angular pointing error on BER performance of underwater optical wireless links," *Opt. Exp.*, vol. 28, no. 23, p. 34606, 2020.

[14] W. C. Cox, J. A. Simpson, C. P. Domizioli, J. F. Muth, and B. L. Hughes, "An underwater optical communication system implementing Reed–Solomon channel coding," in *Proc. Oceans*, Sep. 2008, pp. 1–6.

[15] F. Mattoussi, M. A. Khalighi, and S. Bourennane, "Improving the performance of underwater wireless optical communication links by channel coding," *Appl. Opt.*, vol. 57, no. 9, p. 2115, 2018.

[16] A. Li, P. Wang, W. Pang, W. Chen, S. Liu, and L. Guo, "ABER performance investigation of LDPC-coded multi-hop parallel underwater wireless optical communication system," *Appl. Opt.*, vol. 59, no. 5, p. 1353, 2020.

[17] P. N. Ramavath, S. A. Udupi, and P. Krishnan, "Experimental demonstration and analysis of underwater wireless optical communication link: Design, BCH coded receiver diversity over the turbid and turbulent seawater channels," *Microw. Opt. Technol. Lett.*, vol. 62, no. 6, pp. 2207–2216, Jun. 2020.

[18] Y. Fu and Y. Du, "Performance of heterodyne differential phase-shift-keying underwater wireless optical communication systems in gamma-gamma-distributed turbulence," *Appl. Opt.*, vol. 57, no. 9, p. 2057, 2018.

[19] Y. Fu, Q. Duan, C. Huang, Y. Du, and L. Zhou, "Average BER performance of rectangular QAM-UWOC over strong oceanic turbulence channels with pointing error," *Opt. Commun.*, vol. 476, Dec. 2020, Art. no. 126362.

[20] Q. Zhang, D. Yue, and X. Xu, "Generalized transmit laser selection for vertical underwater wireless optical communications over gamma–gamma turbulence channels," *Opt. Exp.*, vol. 31, no. 23, p. 37943, 2023.

[21] I. C. Ijeh, M. A. Khalighi, M. Elamassie, S. Hranilovic, and M. Uysal, "Outage probability analysis of a vertical underwater wireless optical link subject to oceanic turbulence and pointing errors," *J. Opt. Commun. Netw.*, vol. 14, no. 6, pp. 439–453, Jun. 2022.

[22] D. G. M. Mitchell, M. Lentmaier, and D. J. Costello, "Spatially coupled LDPC codes constructed from protographs," *IEEE Trans. Inf. Theory*, vol. 61, no. 9, pp. 4866–4889, Sep. 2015.

[23] S.-Y. Chung, T. J. Richardson, and R. L. Urbanke, "Analysis of sum-product decoding of low-density parity-check codes using a Gaussian approximation," *IEEE Trans. Inf. Theory*, vol. 47, no. 2, pp. 657–670, Jul. 2001.

[24] S. T. Brink, G. Kramer, and A. Ashikhmin, "Design of low-density parity-check codes for modulation and detection," *IEEE Trans. Commun.*, vol. 52, no. 4, pp. 670–678, Apr. 2004.

[25] K. Huang, D. G. M. Mitchell, L. Wei, X. Ma, and D. J. Costello, "Performance comparison of LDPC block and spatially coupled codes over GF(q)," *IEEE Trans. Commun.*, vol. 63, no. 3, pp. 592–604, Mar. 2015.

[26] S. K. Padala and J. D'Souza, "Performance of spatially coupled LDPC codes over underwater acoustic communication channel," in *Proc. Nat. Conf. Commun. (NCC)*, Feb. 2020, pp. 1–5.

[27] J. Thorpe, "Low-density parity-check (LDPC) codes constructed from protographs," *IPN Prog. Rep.*, vol. 42, no. 154, pp. 42–154, 2003.

[28] G. Liva and M. Chiani, "Protograph LDPC codes design based on EXIT analysis," in *Proc. IEEE Global Telecommun. Conf.*, Nov. 2007, pp. 3250–3254.

[29] M. Elamassie and M. Uysal, "Vertical underwater visible light communication links: Channel modeling and performance analysis," *IEEE Trans. Wireless Commun.*, vol. 19, no. 10, pp. 6948–6959, Oct. 2020.

[30] A. A. Farid and S. Hranilovic, "Outage capacity optimization for free-space optical links with pointing errors," *J. Lightw. Technol.*, vol. 25, no. 7, pp. 1702–1710, Jul. 9, 2007.

[31] S. Jaruwatanadilok, "Underwater wireless optical communication channel modeling and performance evaluation using vector radiative transfer theory," *IEEE J. Sel. Areas Commun.*, vol. 26, no. 9, pp. 1620–1627, Dec. 2008.

[32] W. Liu, Z. Xu, and L. Yang, "SIMO detection schemes for underwater optical wireless communication under turbulence," *Photon. Res.*, vol. 3, no. 3, p. 48, 2015.

[33] M. V. Jamali, J. A. Salehi, and F. Akhoundi, "Performance studies of underwater wireless optical communication systems with spatial diversity: MIMO scheme," *IEEE Trans. Commun.*, vol. 65, no. 3, pp. 1176–1192, Mar. 2017.

[34] L. Yang, X. Song, J. Cheng, and J. F. Holzman, "Free-space optical communications over lognormal fading channels using OOK with finite extinction ratios," *IEEE Access*, vol. 4, pp. 574–584, 2016.

[35] O. Korotkova, N. Farwell, and E. Shchepakina, "Light scintillation in oceanic turbulence," *Waves Random Complex Media*, vol. 22, no. 2, pp. 260–266, May 2012.

[36] M. Elamassie, M. Uysal, Y. Baykal, M. Abdallah, and K. Qaraqe, "Effect of eddy diffusivity ratio on underwater optical scintillation index," *J. Opt. Soc. Amer. A, Opt. Image Sci.*, vol. 34, no. 11, p. 1969, 2017.

[37] Y. Ata and Y. Baykal, "Scintillations of optical plane and spherical waves in underwater turbulence," *J. Opt. Soc. Amer. A, Opt. Image Sci.*, vol. 31, no. 7, p. 1552, 2014.

[38] F. Hanson and S. Radic, "High bandwidth underwater optical communication," *Appl. Opt.*, vol. 47, no. 2, p. 277, 2008.

[39] Y. Dong, S. Tang, and X. Zhang, "Effect of random sea surface on downlink underwater wireless optical communications," *IEEE Commun. Lett.*, vol. 17, no. 11, pp. 2164–2167, Nov. 2013.

[40] Y. Li, Y. Zhang, and Y. Zhu, "Capacity of underwater wireless optical links with pointing errors," *Opt. Commun.*, vol. 446, pp. 16–22, Sep. 2019.

[41] D. Divsalar, C. Jones, S. Dolinar, and J. Thorpe, "Protograph based LDPC codes with minimum distance linearly growing with block size," in *Proc. IEEE Global Telecommun. Conf.*, Jul. 2005, p. 5.

[42] X.-Y. Hu, E. Eleftheriou, and D. M. Arnold, "Regular and irregular progressive edge-growth tanner graphs," *IEEE Trans. Inf. Theory*, vol. 51, no. 1, pp. 386–398, Jan. 2005.

[43] T. J. Richardson and R. L. Urbanke, "Efficient encoding of low-density parity-check codes," *IEEE Trans. Inf. Theory*, vol. 47, no. 2, pp. 638–656, Aug. 2001.

[44] A. E. Pusane, A. J. Feltstrom, A. Sridharan, M. Lentmaier, K. Zigangirov, and D. J. Costello, "Implementation aspects of LDPC convolutional codes," *IEEE Trans. Commun.*, vol. 56, no. 7, pp. 1060–1069, Jul. 2008.

[45] J. Pearl, *Probabilistic Reasoning in Intelligent Systems: Networks of Plausible Inference*. San Mateo, CA, USA: Morgan Kaufmann, 1988.

[46] D. J. C. MacKay, "Good error-correcting codes based on very sparse matrices," *IEEE Trans. Inf. Theory*, vol. 45, no. 2, pp. 399–431, Mar. 1999.
[47] A. R. Iyengar, P. H. Siegel, R. L. Urbanke, and J. K. Wolf, "Windowed decoding of spatially coupled codes," *IEEE Trans. Inf. Theory*, vol. 59, no. 4, pp. 2277–2292, Apr. 2013.
[48] N. Ul Hassan, A. E. Pusane, M. Lentmaier, G. P. Fettweis, and D. J. Costello, "Non-uniform window decoding schedules for spatially coupled LDPC codes," *IEEE Trans. Commun.*, vol. 65, no. 2, pp. 501–510, Feb. 2017.
[49] T. A. Tsiftsis, "Performance of heterodyne wireless optical communication systems over gamma-gamma atmospheric turbulence channels," *Electron. Lett.*, vol. 44, no. 5, p. 373, 2008.
[50] S. Navidpour, M. Uysal, and M. Kavehrad, "BER performance of free-space optical transmission with spatial diversity," *IEEE Trans. Wireless Commun.*, vol. 6, no. 8, pp. 2813–2819, Aug. 2007.
[51] M. Chiani, D. Dardari, and M. K. Simon, "New exponential bounds and approximations for the computation of error probability in fading channels," *IEEE Trans. Wireless Commun.*, vol. 24, no. 5, pp. 840–845, May 2003.
[52] V. S. Adamchik and O. I. Marichev, "The algorithm for calculating integrals of hypergeometric type functions and its realization in REDUCE system," in *Proc. Int. Symp. Symbolic Algebr. Comput.*, Jul. 1990, pp. 212–224.
[53] S. Saoudi, M. Troudi, and F. Ghorbel, "An iterative soft bit error rate estimation of any digital communication systems using a nonparametric probability density function," *EURASIP J. Wireless Commun. Netw.*, vol. 2009, no. 1, pp. 1–9, Dec. 2009.
[54] S. Saoudi, T. Ait-Idir, and Y. Mochida, "A novel non-parametric iterative soft bit error rate estimation technique for digital communications systems," in *Proc. IEEE Int. Conf. Commun. (ICC)*, Jun. 2011, pp. 1–6.
[55] P. Poda, S. Saoudi, T. Chonavel, F. Guilloud, and T. Theodore, "Kernel-based performance evaluation of coded QAM systems," in *Proc. 13th African Conf. Res. Comput. Sci. Appl. Math.*, 2016, pp. 182–191.
[56] S. T. Brink, "Convergence behavior of iteratively decoded parallel concatenated codes," *IEEE Trans. Commun.*, vol. 49, no. 10, pp. 1727–1737, Oct. 2001.
[57] Z. Chen, Y. Gu, P. Chen, J. Zhang, and D. Han, "Improved EXIT algorithm based on Gaussian mixture model and its application to LDPC construction in coding cooperative systems with hybrid fading," *IEEE Access*, vol. 8, pp. 49933–49950, 2020.
[58] D. A. Reynolds, "Gaussian mixture models," *Encyclopedia Biometrics*, vol. 741, pp. 659–663, 2009.
[59] W. H. Press, *Numerical Recipes: The Art of Scientific Computing*, 3rd ed. Cambridge, U.K.: Cambridge Univ. Press, 2007.
[60] L. Devroye, "Nonuniform random variate generation," in *Operations Research and Management Science Handbook*, vol. 13. New York, NY, USA: Springer, 2006, pp. 83–121.
[61] M. Elamassie, S. M. Sait, and M. Uysal, "Underwater visible light communications in cascaded gamma-gamma turbulence," in *Proc. IEEE GLOBECOM Workshops*, Dec. 2018, pp. 1–6.

SRAVAN KUMAR PADALA received the B.E. degree in electronics and communication engineering from Osmania University, Hyderabad, in 2008, and the M.Tech. degree in electronics and communication engineering from the National Institute of Technology Calicut, in 2011. He is currently pursuing the Ph.D. degree in electronics and communication engineering with the National Institute of Technology Karnataka, Surathkal, Karnataka, India.

From 2011 to 2016, he was a Assistant Professor with Madanapalle Institute of Technology and Science, Madanapalle, Andhra Pradesh, India.

JOHN D'SOUZA (Member, IEEE) received the Ph.D. degree in electronics and electrical communication engineering from Indian Institute of Technology, Kharagpur, India, in 1998. Since 1998, he has been with the Department of Electronics and Communication Engineering, National Institute of Technology Karnataka, Surathkal, India, where he is currently a Professor. His research interests include digital communication and error control coding.